sustainability

MDPI

Article

Wildfire Impact Assessment in Watersheds of Alberta's Regional Aquatic Monitoring Program

Dayal Wijayarathne [1,*], Tiago Antonio Morais [1], Aprami Jaggi [1], Nicholas Kouwen [2], Michael Wendlandt [1], Tatiana Sirbu [1] and John J. Gibson [3,4]

[1] InnoTech Alberta, 3608-33 St. NW, Calgary, AB T2L 2A6, Canada; tiago.morais@innotechalberta.ca (T.A.M.); aprami.jaggi@innotechalberta.ca (A.J.); michael.wendlandt@innotechalberta.ca (M.W.); tatiana.sirbu@innotechalberta.ca (T.S.)
[2] Civil and Environmental Engineering, University of Waterloo, 200 University Ave W, Waterloo, ON N2L 3G1, Canada; kouwen@uwaterloo.ca
[3] InnoTech Alberta, 3-4476 Markham Street, Victoria, BC V8Z 7X8, Canada; john.gibson@innotechalberta.ca
[4] Global Institute for Water Security, University of Saskatchewan, 11 Innovation Blvd., Saskatoon, SK S7N 3H5, Canada
* Correspondence: dayal.wijayarathne@innotechalberta.ca

Abstract

Wildfire impact on boreal watersheds was assessed across Alberta's Regional Aquatics Monitoring Program (RAMP) domain by integrating multidecadal river, lake, and sediment physical–chemical data with historical wildfire perimeters, polycyclic aromatic hydrocarbon (PAH) indicators, continuous multiparameter sonde records, and pre-/post-fire hydrologic simulations. Site classification, distinguishing reference, industrial, wildfire, and combined influences, was used to enable spatial and temporal comparisons before, during, and after fires. Our synthesis indicated that wildfire acts as an important disturbance that alters watershed connectivity and transport pathways, resulting in shifts in water quality and quantity in surface waters and longer-term adjustments retained in sediments. The interpretation of chemical signatures, including PAHs, was complicated by overlap between areas with wildfire and industrial activities, highlighting cumulative effects and the importance of spatio–temporal context when assessing and quantifying source contributions for long-term resource sustainability. Hydrologic alteration emerged as the dominant downstream wildfire effect, emphasizing the need for long-term continuous monitoring of fire-responsive indicators, in addition to improved assessment of subsurface pathways in wildfire-prone boreal systems.

Keywords: wildfire; water quality; WATFLOOD; PAHs; sediment quality; hydrologic response; boreal watersheds; diagnostic ratios; continuous monitoring; RAMP

Check for updates

Academic Editors: Shimin Tian and Jia Jia

Received: 24 February 2026
Revised: 24 March 2026
Accepted: 31 March 2026
Published: 10 April 2026

Copyright: © 2026 by the authors. Licensee MDPI, Basel, Switzerland. This article is an open access article distributed under the terms and conditions of the Creative Commons Attribution (CC BY) license.

1. Introduction

Wildfires are among the most economically damaging natural hazards globally, with rapidly rising costs; between 2014 and 2023, wildfire events resulted in approximately USD 106 billion in total economic losses and USD 74 billion in insured losses worldwide [1]. In Canada, wildfire-related economic impacts have similarly escalated, culminating in the record-breaking 2023 fire season, during which nearly 5500 fires burned approximately 17.3 million hectares nationwide, and insured losses approached or exceeded CAD 1 billion [2–4]. Several of Canada's most economically damaging wildfire disasters have occurred in Alberta, including the 2011 Slave Lake wildfire, which caused approximately

CAD 700 million in total damages [5], the 2016 Fort McMurray wildfire, resulting in insured losses exceeding CAD 3.7 billion [2], and the 2024 Jasper wildfire, with insured damages estimated at approximately CAD 1.3 billion [6]. However, these estimates largely under-represent impacts on water resources and aquatic ecosystems, despite evidence that wildfire-driven watershed degradation can impose substantial long-term costs through deteriorated source water quality, loss of ecosystem services, and increased drinking water treatment requirements [7]. This under-representation highlights a critical knowledge gap and reinforces the need for integrated assessments of wildfire effects on hydrological systems, particularly in fire-prone regions, such as Alberta.

Wildfires pose a significant risk to domestic, industrial, and irrigation water supply in Alberta. Currently, multiple counties repeatedly fall under fire advisories during the summer months. Having extensive boreal forests, Alberta's landscape undergoes frequent and severe wildfires, with a reported 76,800 fires affecting more than 18.1 million hectares between 1923 and 2023 [8,9]. The annual area burned in Alberta has followed an increasing trend since 1959, with changing weather patterns contributing to extended periods of hot and dry conditions, which have further exacerbated the frequency and intensity of wildfires [10,11]. Historical records also reveal that fire seasons in Alberta are becoming longer, with more days conducive to fire spread and overnight burning [4,5]. As a result, wildfires have an increased potential to inflict devastating effects on the water supply in the forested region of Alberta. A range of water quality impacts arises from wildfire, including increased sediment, nutrient and pollutant loading, and introduction of contaminants, such as ash, heavy metals, organics, and pathogens [12–16].

Intense heat from wildfires is also associated with destabilization of soils, leading to increased erosion and sediment runoff, which contributes to higher turbidity, altered pH levels, and elevated suspended solids [17–19]. Additionally, wildfires release ash and particulate matter that can deposit metals, such as copper and iron [20,21], as well as polycyclic aromatic hydrocarbons (PAHs), that, when stored as sediments and redistributed by erosion, may act as long-term contamination sources [17,21,22]. Long-lasting effects on canopy interception, transpiration, and water flow pathways, as well as microbial activity and nutrient cycling, generally occur, and in the case of high-severity burns, hydrophobic soil layers can arise that limit infiltration [23–25]. Developing effective monitoring strategies to detect and mitigate wildfire-related impacts on water quality and quantity remains a significant challenge, yet it is essential to predict the trajectories of response and recovery, which can guide restoration and management efforts. Moreover, maintaining healthy aquatic ecosystems is fundamental for environmental sustainability, as these systems support biodiversity, regulate biogeochemical cycles, and provide essential ecosystem services.

In Alberta, the Southern Rockies Watershed Program (SRWP) has made notable contributions to the understanding of regional wildfire impacts in foothills–prairie watersheds, including flow regimes [26], sediment production, source and transport [27,28], groundwater contributions to streamflow [29], macroinvertebrate community structure [30], watershed processes and water quality [31,32], and stream pH and temperature variations [33]. At the outset of this study, our objective was to apply similar methodologies to investigate wildfire impacts across Alberta's boreal forest region. The work aimed to leverage archival datasets collected over two decades through the Regional Aquatics Monitoring Program (RAMP), which monitored watersheds affected by oil sands development, including appreciable areas impacted by wildfire. A subset of these monitored lakes included the acid-sensitive lakes, which were sampled annually to assess potential atmospheric deposition effects.

Relatively few studies have examined wildfire impacts in wetland-rich boreal watersheds in Alberta. Accordingly, this study was structured to evaluate wildfire effects within

RAMP-monitored watersheds by (i) first determining whether wildfire disturbance produces measurable changes in surface-water quality, sediment chemistry, and hydrological response, and (ii) subsequently assessing whether these fire-driven responses are distinguishable from those associated with other regional stressors. A complementary objective was to identify the key physical–chemical indicators most sensitive to both immediate and long-term post-fire disturbance. We tested the hypothesis that wildfire-affected watersheds exhibit coherent, source-specific shifts in key water and sediment quality parameters and hydrological behaviour, relative to non-fire-impacted systems. The analysis explicitly evaluated wildfire-driven changes in surface-water quality, sediment chemistry, and hydrological response, while other wildfire-related processes (e.g., soil hydrophobicity and hillslope erosion) were treated as contextual mechanisms rather than directly analyzed variables. This study focused on water quality statistics, PAH source tracking, and hydrologically derived indicators from long-term archival datasets, enabling the assessment of both immediate and cumulative wildfire effects and supporting improved post-fire monitoring, ecosystem-condition assessment, and sustainability evaluation.

2. Materials and Methods

2.1. Study Area and Data Acquisition

A 43,000 km^2 area was selected for investigation, including portions of 25 watersheds that were historically monitored under the RAMP in the lower Athabasca River region of northeastern Alberta (Mackay, Ells, Firebag, Steepbank, Muskeg, Clearwater, Christina, Hangingstone, Horse River, Big Creek, etc.) (http://www.ramp-alberta.org/RAMP.aspx (accessed on 20 March 2024)). This boreal region is characterized by a cold continental climate [34], extensive peatlands [35], glacial lowlands, and incised river valleys [36], which together create diverse hydrological pathways. Many of these watersheds are located within or adjacent to active oil sands operations. The boreal lowlands in the lower Athabasca are naturally prone to wildfire, with peatlands, dry summers, and dense forest cover contributing to recurrent fire activity across many RAMP watersheds [37]. Historical provincial wildfire data show repeated burns in the region (Alberta Wildfire Dashboard-https://experience.arcgis.com/experience/0e45bd0ef9814d5e9ec3f87900a4cfe9 (accessed on 20 March 2024)), underscoring wildfire as an important driver of hydrological and water quality change. The full spatial distribution of monitored watersheds, sampling sites, oil sands development areas, and historical wildfire perimeters in the RAMP area is shown in Figure 1.

The water quality and sediment quality datasets used in this study were downloaded from the RAMP website (https://www.ramp-alberta.org/RAMP.aspx (accessed on 28 March 2024)), which currently provides public access to historical monitoring results, watershed information, and associated metadata. These data include multi-decadal records from the RAMP (1997–2016), supplemented with additional river chemistry information from the Long-Term River Network (LTRN). The RAMP sediment data and records from the acid-sensitive lakes program were also incorporated to characterize long-term depositional and metal chemistry trends. Historical and geospatial wildfire datasets covering 1931–2023 were obtained from the Government of Alberta wildfire data portal (https://www.alberta.ca/wildfire-maps-and-data (accessed on 28 March 2024)), providing the temporal and spatial context required to link wildfire occurrence with observed water quality and hydrological responses.

Although the RAMP website remains accessible at present, it is an unsupported legacy platform and will be permanently decommissioned in early 2026, with all program content—including monitoring databases, watershed pages, and downloadable files—archived in the Oil Sands Monitoring (OSM) Data Catalogue (https://osmdatacatalog.

alberta.ca/pubdata/ramp-website (accessed on 20 December 2025)) for long-term public access. This ensures that readers wishing to verify or access RAMP datasets in the future will find them preserved within the OSM system.

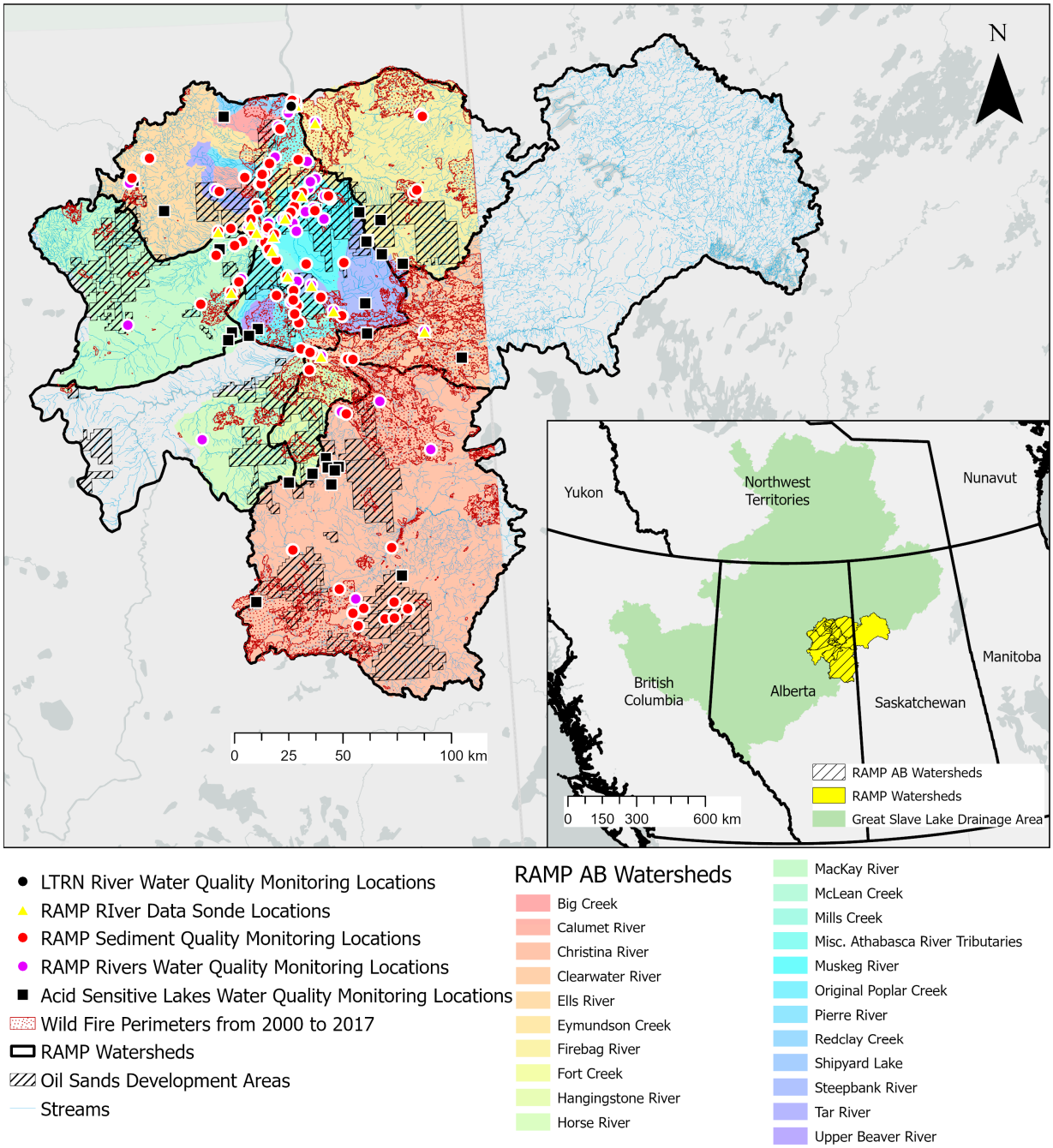


Figure 1. The study area map showing RAMP watersheds, RAMP, LTRN and acid-sensitive lakes monitoring locations, oil sands development areas, and historical wildfire perimeters in the lower Athabasca region of northeastern Alberta.

2.2. Data Processing and Standardization

Water and sediment quality data from the RAMP and the LTRN databases were compiled and processed before analysis. Data cleaning involved multiple steps to ensure consistency, accuracy, and comparability across the dataset. One key step was the removal of values reported as below detection limit (e.g., "<0.01"). These values do not represent precise quantitative measurements but rather indicate concentrations below the analytical

detection capability of the instrument. Because this study focused on concentration shifts and anomalies, assigning a fixed replacement value to these observations could misrepresent true concentrations and introduce artificial variation into the analysis. These records were therefore excluded. This decision reduces the risk of bias associated with arbitrary substitution, but it may also limit the representation and interpretation of low-concentration signals near background levels.

Additionally, when multiple columns representing the same parameter were identified but reported in different units, these values were standardized to a common unit and combined into a single dataset. This step was necessary to ensure uniformity across monitoring locations and to facilitate direct comparisons of water and sediment quality parameters. Through these preprocessing steps, the dataset was refined and structured appropriately for subsequent classification and analysis.

2.3. Site Classification

A site classification system was developed for each water and sediment quality monitoring location to evaluate potential influences from oil sands-related activities and wildfire. A 500 m radius buffer was created around each monitoring location as a standardized spatial and methodological criterion for identifying nearby oil sands-related and wildfire disturbances. This buffer was intended to capture disturbances immediately adjacent to each site that could plausibly influence water and sediment quality, particularly for locations within lakes or large rivers, where a point-based approach alone would not detect nearby shoreline or land-based stressors. Applying a uniform 500 m buffer provided a consistent and conservative basis for classification while reducing the likelihood of overlooking proximal disturbances. However, this threshold should be interpreted as an operational classification criterion rather than a definitive ecological boundary of impact. Geospatial data from all monitoring locations were combined with fire perimeter datasets and mapped oil sands project areas to determine the presence of these environmental stressors within each buffer. Based on this information, monitoring locations were classified into four distinct categories: reference (R), oil sands (OSs), oil sands and wildfire (OSs&WF), and wildfire (WF).

Reference sites were those where neither wildfire nor industrial activities were present within the 500 m buffer, serving as baseline locations and assumed to be unaffected by these disturbances. Oil sands sites were characterized by the presence of industrial activities related to oil sands development within the buffer but assumed to have no evidence of wildfire impacts. The oil sands and wildfire category included sites where both oil sands-related activities and wildfire disturbances occurred within 500 m of the monitoring location. Finally, Wildfire sites were those where wildfire activity was documented within the buffer but assumed to have no industrial development impacts present. This classification system provided a structured approach to distinguish potential environmental influences on water and sediment quality across the study area.

Following this classification, wildfire geospatial data were extracted to identify the year of the fire for each affected monitoring location. This information allowed for a more detailed assessment of wildfire impacts on water and sediment quality by distinguishing between pre-fire, active fire, and post-fire conditions. Incorporating temporal wildfire data enabled a more comprehensive evaluation of potential changes in water and sediment quality over time in relation to fire events.

2.4. Water and Sediment Quality Data Analysis

To ensure a comprehensive analysis, a subset of parameters was carefully selected based on an extensive literature review and preliminary data investigations [38]. All

available parameters in the historical datasets were initially examined using exploratory plots. Parameters were then prioritized based on (i) relevance identified in the literature, (ii) sufficient data availability across monitoring locations and time periods, and (iii) evidence from preliminary evaluation that the parameter showed meaningful variation or response patterns relevant to the study objectives. This selection approach was used to identify the most informative indicators of potential impacts while reducing bias associated with sparse or uninformative variables. Different parameters were selected for water and sediment samples based on their relevance to each matrix. The selected parameters included physical–chemical indicators, metals, and PAHs. Specifically, key physical–chemical parameters, such as dissolved oxygen (DO), phosphorus, total suspended solids (TSSs), pH, and turbidity were chosen for water quality samples, while calcium, total organic carbon (TOC), grain size, and moisture were prioritized for sediment samples. Heavy metals, such as arsenic, cadmium, copper, and zinc, were selected for both matrices, and PAH compounds, including benzo[a]pyrene, fluoranthene, and pyrene, were included for both water and sediment samples. This approach aimed to capture the most relevant indicators of potential impacts while maintaining consistency across the data. The complete set of parameters considered for water and sediment samples can be visualized in the plots presented in the results section, with further details available in Table S1.

In order to visualize wildfire impacts, box plots of the selected parameters were generated based on the site classification. Data from the entire monitoring period were used for each monitoring location. The box plots represent the distribution of each parameter across the different site classifications. In the box plots, the central line within the box indicates the median, the box itself represents the interquartile range (from the 25th to 75th percentiles), and the whiskers extend to the highest and lowest values within 1.5 times the interquartile range. Data points outside this range were considered outliers and were included in the analysis. The *y*-axis of the box plots was displayed on a logarithmic scale to better illustrate the variability in the data and ensure that outliers were clearly visible. While the median provides insight into the long-term impacts potentially associated with wildfires and industrial activities, outliers may indicate short-term impacts. Therefore, the frequency of outliers is a critical piece of information for this specific study.

Given that wildfires affected only a short period compared to the overall duration of the monitoring period, it is likely that the impacts are highly diluted. To address this, additional box plots were created for monitoring sites, specifically their relationship to the time elapsed since fire. The data was separated into time before, during, 1 year after, 2 years after, and 3+ years after fire to allow for a more focused analysis of the impact of wildfire over time.

2.5. Water Quality Sonde Data

To evaluate the potential for the early detection of wildfires through continuous water quality monitoring, we examined short-term variations in time series data collected using water quality sondes. The parameters selected for this investigation included dissolved oxygen, pH, conductivity, and turbidity. Data from two sites were analyzed during a wildfire event to assess whether continuous monitoring of these parameters could provide an early indication of its occurrence. This analysis was limited to two sites because continuous sonde records were only available for these locations during the wildfire event, and the results should, therefore, be interpreted as an initial assessment rather than a broadly generalizable conclusion regarding early wildfire detection. These parameters were specifically chosen for their sensitivity to changes that often follow wildfire, as well as their ability to detect disturbances in water quality that may result from wildfire activity. By investigating

these parameters, we aimed to determine if continuous water quality data could provide valuable insights for early wildfire detection and monitoring.

The analysis aimed to assess whether changes in commonly measured water quality parameters could reliably signal the presence of a wildfire, as suggested by previous studies [18,38]. Building on these previous investigations, we leveraged data from water quality sondes for continuous monitoring across a large area to evaluate whether such broad-scale data could effectively detect wildfire-related impacts. This approach not only supports previous conclusions but also enhances our understanding of how wildfires affect aquatic ecosystems. With this comprehensive dataset, we have the potential to assess the accuracy and efficiency of continuous monitoring for large-scale applications, providing valuable insights for early detection of wildfire impacts.

2.6. PAH Source Tracing

Polycyclic aromatic hydrocarbons (PAHs) are a class of organic compounds that are composed of two or more aromatic (benzene) rings that are fused together, consisting solely of carbon and hydrogen atoms. PAHs are generated during wildfires as a result of the incomplete combustion of organic material, including vegetation, wood, and soil organic matter. Based on the number of rings present in the compounds, PAHs are classified into light-molecular-weight PAHs (LMW PAHs; having two or three fused aromatic rings) and high-molecular-weight PAHs (HMW PAHs; having four or more fused aromatic rings). This structural distinction impacts the physical characteristics of the PAHs and can be used to define types of PAH sources. PAH molecules with only cyclic structures are referred to as 'Parent PAHs', and the PAHs with alkyl substituents, such as methyl and ethyl groups, are referred to as 'Alkylated PAHs'. PAHs are classified as toxic, persistent, and bioaccumulative contaminants, with exposure linked to adverse reproductive outcomes, respiratory disorders, cardiotoxicity, immunotoxicity, neurotoxicity, and an increased risk of various cancers, posing significant threats to both human health and the environment [39–41]. The Canadian Council of Ministers of the Environment (CCME) has a list of 13 parent PAHs outlined in the water quality guidelines for the protection of aquatic life [42].

Wildfires are not the only source of PAHs in the environment. Based on their origin and formation mechanisms, PAHs are categorized as either pyrogenic, petrogenic or biogenic. Pyrogenic PAHs are generated through high-temperature combustion, incomplete combustion, and/or pyrolysis of organic matter under oxygen-deficient or anoxic conditions. These processes occur in various combustion sources, including fossil fuel combustion, biomass burning (e.g., wood and wildfires), coal combustion, and volcanic activity [43]. Petrogenic PAHs are derived from natural hydrocarbon deposits, such as coal, bitumen sands, crude oil, and natural gas, which have been formed over millions of years through geological processes. These hydrocarbons undergo thermal maturation under high-pressure conditions and relatively low-temperature regimes driven by non-intrusive geothermal heat, resulting in the generation and accumulation of PAHs within sedimentary deposits [43]. Biogenic PAHs are formed through the degradation of vegetative organic substances by plants, algae, and microorganisms or during the slow transformation of organic material in soils by plants and microbes [44–47].

The identification of PAH sources is particularly challenging when multiple inputs of similar origin contribute to environmental contamination. The diverse anthropogenic and natural sources of PAHs can be characterized by analyzing their compositional patterns within sample matrices. Within the region of current investigation, wildfires and oil sands activities represent the two primary sources of PAHs in the environment. To assess the impact of wildfire on water resources, it is essential to differentiate between these

contributing sources. The RAMP and LTRN datasets were analyzed to assess diagnostic PAH ratios for potential source apportionment through widely used approaches, such as the application of diagnostic ratios and double-ratio plots to classify samples based on specific indicator PAHs (investigated in further detail in Section 3.5 [44,48–51].

2.6.1. Relative Concentrations of Parent Versus Alkylated PAHs

The relative distribution of parent versus alkylated PAHs can serve as a useful indicator for distinguishing between pyrogenic and petrogenic PAHs [44,51]. The high combustion temperatures (such as in wildfires) associated with the generation of pyrogenic PAHs facilitate the thermal degradation of alkyl side chains, resulting in a lower relative abundance of alkylated compounds. In contrast, petrogenic PAHs undergo diagenetic and thermogenic processes over geological time, leading to a higher degree of alkylation.

2.6.2. Diagnostic Ratios

Low-temperature combustion processes result in the formation of LMW PAHs, while HMW PAHs are produced during high-temperature processes (such as wildfire). At higher temperatures, the organic carbon produces reactive radicals to form less-alkylated pyrogenic PAHs, relative to petrogenic PAHs [51,52]. Diagnostic ratios leverage these differences in the parent versus alkylated PAH distribution patterns and converts it to a numeric form. Several such diagnostic ratios have been recommended in the existing literature. In this study, we use the pyrogenic index (PI), ratios of fluoranthene/(fluoranthene + pyrene) [Fla/(Fla + Pyr)], retene/(retene + chrysene) [Ret/(Ret + Chy)], and a cross-plot of benzo(a)anthracene/(benzo(a)anthracene + chrysene) versus fluoranthene/(fluoranthene + pyrene) [BaA/(BaA + Chy) vs. Fla/(Fla + Pyr)] to distinguish between pyrogenic and petrogenic sources at RAMP and LTRN sites.

The pyrogenic index (PI) is defined as the ratio of selected 3–6 ring parent PAHs to the total of 5 target alkylated PAH homologues [51,53,54] and has proven useful for differentiation of pyrogenic and petrogenic PAHs [53,54]. The index leverages these differences in the parent versus alkylated PAH distribution patterns and converts them to a numeric form. The PI was calculated in this study using the following equation (abbreviations are outlined in Table 1):

$$\mathrm{PI} = \frac{(\mathrm{Acy} + \mathrm{Ace} + \mathrm{Ant} + \mathrm{Fla} + \mathrm{BaA}(+\mathrm{BeP} + \mathrm{BghiP} + \mathrm{IcdP} + \mathrm{DahA})}{\mathrm{NaP}(1-4) + \mathrm{Phen/Ant}(1-4) + \mathrm{D}(1-4) + \mathrm{Fl}(0-4) + \mathrm{Chr}(0-4)} \quad (1)$$

The PI typically ranges from 0.8 to 2.0 for pyrogenic sources, whereas significantly lower values have been reported for petrogenic sources, with <0.01 for crude oils and <0.05 for heavy oils and fuels [51]. This is due to the predominance of HMW PAHs (4–6 ring compounds) over LMW PAHs (2–3 ring compounds) in pyrogenic sources.

The use of diagnostic PAH ratios for source apportionment between pyrogenic and petrogenic sources is subject to limitations, as this approach assumes that the relative proportions of PAH compounds in each source are distinct and that these proportions remain stable as they are transported through the environment [49,55,56]. Despite these constraints, diagnostic ratios can provide valuable insight into compositional differences among PAH sources.

2.7. Hydrological Modelling

Hydrological modelling was used to examine how wildfire disturbance influences watershed hydrological behaviour by comparing conditions before and after wildfire occurrence. Under this paired-scenario framework, pre-fire conditions represent undisturbed land cover, while post-fire scenarios incorporate wildfire-affected land-cover changes, with

all other model components held constant to enable direct attribution of hydrological change to wildfire disturbance. This paired comparison allows wildfire-related changes in streamflow response to be evaluated independently of other confounding factors, such as climate variability or model recalibration. Within this context, wildfire impacts are expected to alter runoff generation processes, leading to measurable changes in hydrograph characteristics, such as flow magnitude, timing, and recession behaviour at the event scale [57–61].

Table 1. List of PAHs and abbreviations used in this manuscript.

PAH Name	Abbreviation	# Bezene and Total Rings
Naphthalene	NaP	2
C2-Naphthalene	NaP2	2
C3-Naphthalene	NaP3	2
C4-Naphthalene	NaP4	2
Acenaphthalene	Acy	2
Acenaphthene	Ace	2
Fluorene	Fl	2
C1-Fluorene	Fl1	2
C2-Fluorene	Fl2	2
C3-Fluorene	Fl3	2
C4-Fluorene	Fl4	2
C1-Dibenzothiophene	D1	2
C2-Dibenzothiophene	D2	2
C3-Dibenzothiophene	D3	2
C4-Dibenzothiophene	D4	2
Phenanthrene	Phe	3
Anthracene	Ant	3
C1-Phenanthrene/anthracene	Phe/Ant1	3
C2-Phenanthrene/anthracene	Phe/Ant2	3
C3-Phenanthrene/anthracene	Phe/Ant3	3
C4-Phenanthrene/anthracene	Phe/Ant4	3
Fluoranthene	Fla	3
Pyrene	Pyr	4
C1-Fluoranthene/pyrene	Fla/Pyr1	4
C2-Fluoranthene/pyrene	Fla/Pyr2	4
C3-Fluoranthene/pyrene	Fla/Pyr3	4
Benz(a)anthracene	BaA	4
Chrysene	Chr	4
C1-Chrysene	Chr1	4
C2-Chrysene	Chr2	4
C3-Chrysene	Chr3	4
C4-Chrysene	Chr4	4
Benzo(b,j,k)fluoranthene	BbjkF	4
Benzo[a]pyrene	BaP	5
Dibenz(a,h)anthracene	DahA	5
Indeno(1,2,3-cd)pyrene	IcdP	5
Benzo(g,h,i)perylene	BghiP	6

The paired pre- and post-fire scenario framework was implemented with WATFLOOD®/CHARM® [62], a distributed rainfall–runoff model in which Grouped Response Units (GRUs) [63] link hydrological parameters directly to land-cover classes. Because wildfire impacts are expressed primarily as land-cover change—loss of canopy, altered ground cover and roughness, reduced interception, and modified shallow storage—these effects were represented by updating the GRU classes while keeping the hydrological param-

eters for each GRU class unchanged, thereby avoiding ad hoc retuning and preserving physical interpretability. This modelling strategy ensures that simulated pre-/post-fire differences reflect primarily land cover disturbance rather than recalibration effects. The WATFLOOD®/CHARM® is scalable and computationally efficient, with a long record of operational use across Canadian basins—such as Manitoba Hydro, Environment and Climate Change Canada, Parks Canada, and multiple conservation authorities, including Grey Sauble, Kettle Creek, Saugeen Valley, and Nattawasaga Valley [64]. This pedigree enables large-domain, scenario-based experiments to run at practical runtimes. Integration with Green Kenue™ [65] provides grid generation, visualization, and routing diagnostics, making the system well-suited to quantify fire-related hydrologic shifts in a physically interpretable and spatially explicit manner.

2.7.1. Model Architecture and Implementation

Within WATFLOOD®/CHARM®, a structured workflow was applied in which topography, land cover, and disturbance (fire perimeter) layers were integrated to support paired pre- and post-fire simulations. Core inputs included a Digital Elevation Model (DEM) for channel and basin delineation, land-use/land-cover (LULC) products for GRU definition, and burn-perimeter overlays to construct the pre-fire and post-fire scenario files. This consistent architectural setup across scenarios supports direct comparison of pre- and post-fire hydrological behaviour. The Medium Resolution Digital Elevation Model (MRDEM) [66] provided the terrain framework and guided the extraction of the drainage network that served as the routing backbone. Channel networks and watershed boundaries were generated using Green Kenue™, while GRUs were derived from Natural Resources Canada (NRCan) land-cover products [67,68], ensuring that hydrologic parameters remained explicitly tied to spatially distributed land-surface classes. The model included nine major types of GRUs: grassland (regeneration–young emergent vegetation), coniferous forest, deciduous forest, mixed wood forest, shrubland, barren land, connected wetlands, treed wetlands, and open water. This architecture allowed both scenarios to be executed under a consistent hydrologic parameterization, ensuring that differences in modelled behaviour reflected land-cover disturbance rather than parameter drift.

To balance computational efficiency with spatial fidelity, several grid resolutions were evaluated. A coarse ~10 km (~100 km^2 cell area) grid was used initially for rapid domain screening and some preliminary model runs for familiarization with the domain. A refined ~3 km working grid (~9 km^2 cell area) was then adopted for full production runs, with grid alignment and cell dimensions selected to keep the domain within a manageable size (~5000 cells). This end-to-end configuration provided a stable, portable modelling environment in which GRU-based parameters could be transferred consistently across basins, while enabling clear attribution of hydrologic changes to wildfire-driven land-cover modification.

2.7.2. Hydrometeorological and Hydrometric Data

Meteorological forcings comprised Regional Deterministic Precipitation Analysis-Canadian Precipitation Analysis (RDPA–CaPA) [69] precipitation and Regional Deterministic Prediction System (RDPS) one-day-ahead temperature at ~10 km resolution. Historical Environment and Climate Change Canada (ECCC) station series were reviewed against these gridded products, but given declining gauge density and the undersampling of short, intense storms, RDPA/RDPS were adopted as the primary inputs. Streamflow evaluation drew on Water Survey of Canada (WSC) observations. From the many gauges in the domain, only ten stations could be used for domain-wide tests on coarse grids (~10 km), where their modelled drainage areas aligned with WSC contributing-area meta-

data. To accommodate all WSC gauges, a 3 km grid was required (full station details in Supplementary Materials Table S2). These observational data provide the basis for model calibration, validation, and subsequent performance evaluation used to support hydrological inference.

2.7.3. Model Parameter Optimization

Model calibration and evaluation were undertaken to ensure that simulated streamflow magnitude, timing, and water-balance behaviour were reproduced with acceptable skill prior to applying the pre-/post-fire scenario analysis. The optimization workflow was staged, beginning with an initial coarse, rapid, domain-wide screening (Stage 1), followed by production–grid calibration (Stage 2), then focused sub-domain refinement (Stage 3), and concluding with a whole-domain run (Stage 4), using narrowly constrained bounds. This staged approach enabled the early identification of structural and data issues, directed search effort where it was most effective, and produced a consolidated, transferable parameter set suitable for simulations across the full calibration period. The initial ~10 km domain was abandoned as soon as it became apparent that too many WSC gauges would be unusable. Production calibration on the ~3 km grid (Stage 2) then applied GRU-aware optimization, using class-specific diagnostics to progressively narrow parameter ranges. Spatially coherent biases revealed by these diagnostics motivated targeted sub-domain calibration across hydrologically similar regions (Stage 3), allowing focused refinement of runoff generation, storage, snowmelt, recharge, and routing parameters. A final (Stage 4) consolidation merged transferable sub-domain values and executed a last narrow-bound optimization run to produce a unified parameter set for the optimization period.

Calibration was performed for 2015–2022 using RDPA–CaPA precipitation and RDPS temperature as the primary hydrometeorological forcings, with WSC streamflow as the observational reference. This combination ensured spatially continuous meteorological inputs and standardized discharge records across the domain. To assess sensitivity to forcing choice during years with comparatively denser station coverage, supplementary 2015–2018 simulations were also conducted using Regional Deterministic Reanalysis System (RDRS) forcings and ECCC climate station series where available, confirming that the CaPA–RDPS-driven calibration was not dependent on a single forcing product.

The parameter optimization employed the Dynamically Dimensioned Search (DDS) algorithm [70] within OSTRICH [71], using the Kling–Gupta Efficiency (KGE) (Equation (2)) [72,73] as the objective function, supported by two complementary diagnostics—the Nash–Sutcliffe Efficiency (NSE) (Equation (3) [74] and volumetric error (Dv %) (Equation (4)) [75]—to distinguish timing and variability performance from long-term water-balance bias.

$$\mathrm{KGE} = 1 - \sqrt{(\mathrm{r}-1)^2 + (\beta-1)^2 + (\gamma-1)^2} \tag{2}$$

$$\mathrm{NSE} = 1| \ \ - | \ \frac{\sum_{t=1}^{T}(Q_{obs,t} - Q_{sim,t})^2}{\sum_{t=1}^{T}(Q_{obs,t} - \mu_{obs})^2}, \tag{3}$$

$$\mathrm{Dv}(\%) = \left(\frac{\sum_{t=1}^{T} Q_{sim,t} - \sum_{t=1}^{T} Q_{obs,t}}{\sum_{t=1}^{T} Q_{obs,t}}\right) \times 100 \tag{4}$$

$$\mathrm{r} = \frac{\sum_{t=1}^{T}\left(Q_{sim,t} - \overline{Q}_{sim}\right)\left(Q_{obs,t} - \overline{Q}_{obs}\right)}{\sqrt{\sum_{t=1}^{T}(Q_{sim,t} - \overline{Q}_{sim})^2}\sqrt{\sum_{t=1}^{T}(Q_{obs,t} - \overline{Q}_{obs})^2}}, \tag{5}$$

where

r(Equation(5)) = Pearson's linear correlation (Equation (4)) between simulated and observed streamflow.

$\beta = \mu_{sim}/\mu_{obs}$: mean (bias) ratio.

$\gamma = (\sigma_{sim}/\mu_{sim})/(\sigma_{obs}/\mu_{obs})$: relative variability ratio.

μ_{sim}, μ_{obs}: mean simulated and observed streamflow.

σ_{sim}, σ_{obs}: standard deviation of simulated and observed streamflow.

$Q_{sim,t}$: simulated streamflow at time t.

$Q_{obs,t}$: observed streamflow at time t.

$\overline{Q}_{sim}$, $\overline{Q}_{obs}$: mean simulated and observed streamflow over period T.

T: total number of time steps in the calibration period.

Summations $\sum_{t=1}^{T}$ represent total simulated or observed discharge accumulated over the calibration period.

Throughout the workflow, GRU error–area slopes, drainage-area trends in Dv% and KGE, and hydrograph evaluations ensured that improvements were physically consistent across land-cover classes and scales. Final parameters were selected based on near-zero GRU error slopes, preserved or improved KGE without worsening Dv%, and the absence of station-specific artifacts, with only minor localized adjustments where lake or routing influences required them. The outcome is a single, transferable calibration suitable for domain-wide application. These metrics were used to evaluate model performance and confirm suitability for interpreting wildfire-driven hydrological change.

2.7.4. Wildfire Disturbance Modelling

Wildfire disturbance was evaluated using two configurations in the RAMP watersheds, including the 2016 Horse River "The Beast" (Fort McMurray) Wildfire (2015 pre-fire; 2020 post-fire, Figure S1), to quantify changes in runoff (surface-water response) and the Baseflow Index (BFI) (groundwater contribution) [76] as indicators of wildfire effects. The 2020 setup reclassified unrecovered burn areas to "regeneration" GRUs, parameterized with the model's grassland settings—lower canopy interception, reduced root-zone storage, and greater quick flow propensity consistent with early-successional cover—while unburned areas retained the 2015 parameters. Meteorological forcings and routing were held constant across scenarios, so only LULC-driven parameters and GRU fractions differed. The BFI was computed over matched analysis windows as the ratio of grid groundwater outflow to the total grid outflow to the river (i.e., river flow leaving the grid cell), alongside scenario comparisons of runoff (Equation (6)).

$$\mathrm{BFI} = \frac{\sum_{t=1}^{T} Q_{gw}(t)}{\sum_{t=1}^{T} Q_{tot}(t)} \tag{6}$$

where

$Q_{gw}(t)$: the groundwater outflow from the grid to the river (slow–reservoir/groundwater discharge) at day t.

$Q_{tot}(t)$: the total river outflow leaving the grid cell at day t(groundwater/baseflow + quickflow/surface and near-surface contributions).

T: the number of daily time steps in the analysis window.

3. Results and Discussion

3.1. Wildfire Impacts on Water Quality

3.1.1. River Monitoring Locations

Wildfire-affected sites (OSs&WF and WF) exhibit larger bias in the frequency of upper outliers (values exceeding 1.5 times the interquartile range above Q3) for several physical–chemical parameters compared to the reference sites (R) (Figure 2A; Table S3). For example,

OSs&WF locations exhibited 2.1 times more phosphorus upper outliers, and WF sites had 2.4 times more TSS upper outliers. Some outliers were more than two orders of magnitude higher or lower, particularly for DO, where WF locations had a six times greater number of lower outliers (values below 1.5 times the interquartile range below Q1) compared to the reference sites. Turbidity and conductivity followed similar trends, with an increase in the frequency of upper outliers at wildfire-impacted sites. These patterns indicate greater variability and a higher occurrence of extreme values at wildfire-affected sites, consistent with more episodic or short-term responses. In addition, significant increases (>25%) in the median values for phosphorus, TSSs, and turbidity were observed at these monitoring locations. In contrast to outlier frequency, these shifts in median values suggest broader changes in the central tendency of water quality conditions. Together, these results indicate that wildfire-affected sites differ from reference sites in both the frequency of extreme observations and the overall distribution of some parameters, although these metrics reflect different types of environmental response. These findings align with previous studies that have suggested that while wildfire impacts can be transient for some parameters, others may be affected for much longer periods [18,38].

Wildfire impacts were also evident in the concentrations of several dissolved metals, with OSs&WF and WF sites showing increased median values and a higher frequency of upper outliers compared to the reference sites (R) (Figure 2B; Table S3). This relationship was particularly pronounced for selenium, nickel, and cadmium, which exhibited the highest increases in median values. At OSs&WF sites, selenium increased by 2.5 times, nickel by 1.8 times, and cadmium by 1.8 times compared to the reference sites, with similar increases at WF sites. Additionally, selenium and nickel showed the most significant rise in upper outliers, while cadmium, zinc, and lead saw concentrations spiking more than three orders of magnitude higher than typical levels. These extreme increases in concentration, coupled with the rise in median values, suggest that wildfires may be associated with short-term spikes in metal concentrations but may also contribute to more lasting impacts on river water quality. These findings are consistent with numerous studies reporting elevated metal concentrations in rivers following wildfires [18,21,22], driven by erosion, deposition, and the mobilization of contaminants from burned landscapes. Notably, despite the relatively dilute nature of this dataset, changes in median values were still observed, indicating that wildfire-related impacts on metal concentrations are detectable and may persist over time.

Finally, increases in both median concentrations and the frequency of upper outliers for several PAHs were observed at sites impacted by oil sands extraction and wildfires compared to the reference sites (Figure 2C; Table S3). The most notable changes were in chrysene, fluoranthene, and benzo[a]pyrene, which showed some of the highest increases in both medians and upper outlier frequencies. At OSs&WF sites, chrysene concentrations were over 2.5 times higher than the reference sites, fluoranthene was nearly 1.5 times higher, and benzo[a]pyrene increased by approximately 1.6 times. Alongside these shifts in medians, the number of upper outliers for several PAHs rose significantly at both OSs&WF and WF sites. For instance, chrysene had more than 2 times the number of upper outliers at WF sites compared to the reference sites, with retene, fluoranthene, and pyrene also showing very elevated outlier frequencies at OSs&WF and WF sites. This increase in both medians and outliers suggests that wildfires, alongside oil sands extraction, contribute to both immediate spikes and potentially lasting changes in PAHs concentrations. These results align with previous studies that report elevated PAH levels in aquatic systems after wildfires, due to factors that control the transport of metals [21,22]. Accordingly, the observed shifts in PAH concentrations are consistent with wildfire-related and industrial influences, including their possible combined effects, rather than wildfire effects alone.

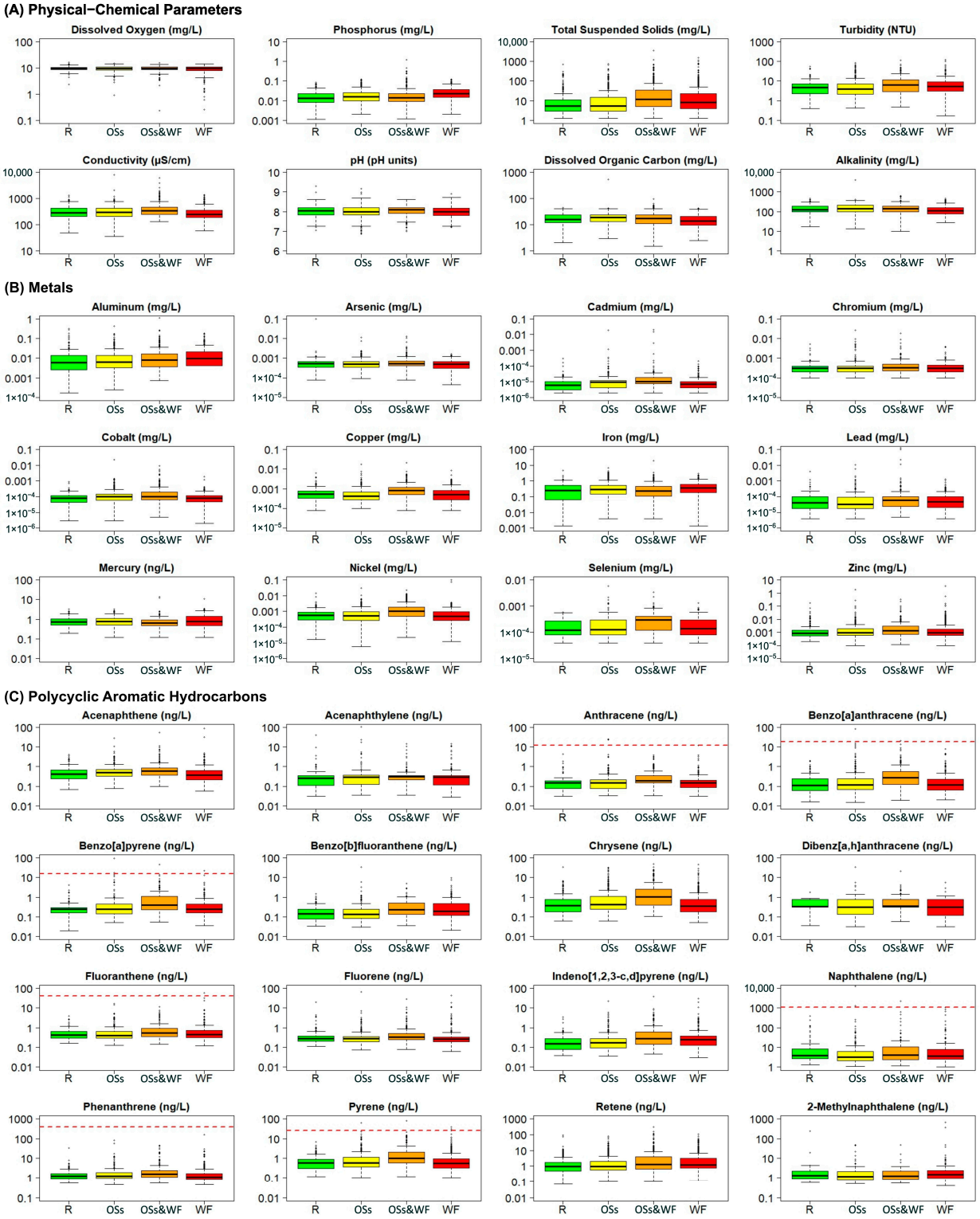


Figure 2. Box plots showing the distribution of physical–chemical parameters, metals, and PAHs for water samples, categorized by site classification (R = reference, OSs = oil sands, OSs&WF = oil sands and wildfire, and WF = wildfire). The central line indicates the median, the box represents the interquartile range, and the whiskers extend to values within 1.5 times the interquartile range. Outliers are shown as data points outside this range. The *y*-axis is on a logarithmic scale, and the PAH guideline values are indicated by the red dashed line (when available).

3.1.2. Acid-Sensitive Lakes Monitoring Locations

Samples from acid-sensitive lakes were limited in the number of parameters measured compared to river monitoring sites. While river samples included PAH data, lake samples lacked this information, and a smaller number of physical–chemical parameters and metals were evaluated. Additionally, no monitoring site had both OSs and WF influence at the same time (OSs&WF), so the analysis was limited to three classes. Despite these constraints, some trends observed in the acid-sensitive lakes were similar to those found in the river samples (Figure S2A).

In acid-sensitive lakes impacted by wildfires, significant changes were observed in both physical–chemical parameters and metal concentrations compared to reference sites (Figure S2; Table S7). Physical–chemical parameters showed notable increases, with conductivity at WF sites being nearly 2 times higher than at the reference sites, and pH increasing by about 1.1 times at WF locations. Turbidity at WF sites was also about 1.2 times higher compared to the reference sites, suggesting that wildfires exacerbate sediment mobilization in the vicinity of these locations. Additionally, phosphate and TSSs exhibited moderate changes in median values, and both showed an increased frequency of upper outliers at WF sites. These shifts in water quality are consistent with similar patterns observed in river samples, suggesting that lakes, like rivers, experience both immediate and lasting disturbances from wildfires.

For metals, although median concentrations did not differ significantly between impacted and reference sites, there was a marked increase in the frequency of upper outliers for several metals at both the OSs and WF sites (Figure S2B; Table S7). For example, dissolved aluminum at the WF monitoring locations showed 7.6 times the number of upper outliers compared to the reference sites, while vanadium exhibited more than 12 times as many upper outliers. Nickel concentrations at the WF sites were 1.25 times higher, but again, the significant shift was in the frequency of outliers. Overall, dissolved metals in acid-sensitive lakes showed slightly lower median concentrations compared to reference sites. However, the substantial increase in the frequency of upper outliers indicates notable short-term spikes in dissolved metal concentrations, especially at the WF sites. Despite the lack of significant shifts in median concentrations for most metals, the increased frequency of upper outliers suggests that wildfire may be associated with episodic metal mobilization in these areas, leading to short-term spikes in dissolved metal concentrations rather than a broad shift in overall concentrations.

3.2. Wildfire Impacts on Sediment Quality

Significant decreases were observed in the median values for calcium, TOC, TIC, moisture, and clay content in sediment samples collected at the wildfire-affected sites compared to the reference sites (Figure 3A; Table S4). For example, calcium levels were more than 5 times lower at both the WF sites compared to the R sites. TOC and moisture content also exhibited notable reductions, with TOC at the WF and OSs&WF sites being more than 1.5 times smaller than at the R sites, and the moisture content reduced by more than 1.2 times compared to the WF sites. These reductions suggest that erosion may be occurring at these locations, likely driven by wildfire-induced disturbances. The loss of calcium and organic matter, alongside decreases in clay content (up to 2 times), may reflect soil degradation and increased mobilization of sediment, possibly linked to enhanced runoff and soil instability following the wildfires. In contrast, potassium levels remained relatively stable throughout the sampling periods, with a slight decrease in median at both the WF and OSs&WF sites compared to the R sites, indicating its concentration was less influenced by long-term wildfire impacts compared to other parameters. Other studies have also indicated that wildfire disturbances can lead to significant changes in soil properties,

with increases in erosion and mobilization of finer particles contributing to changes in soil chemistry, physical properties, and water infiltration rates [17,38,77,78].

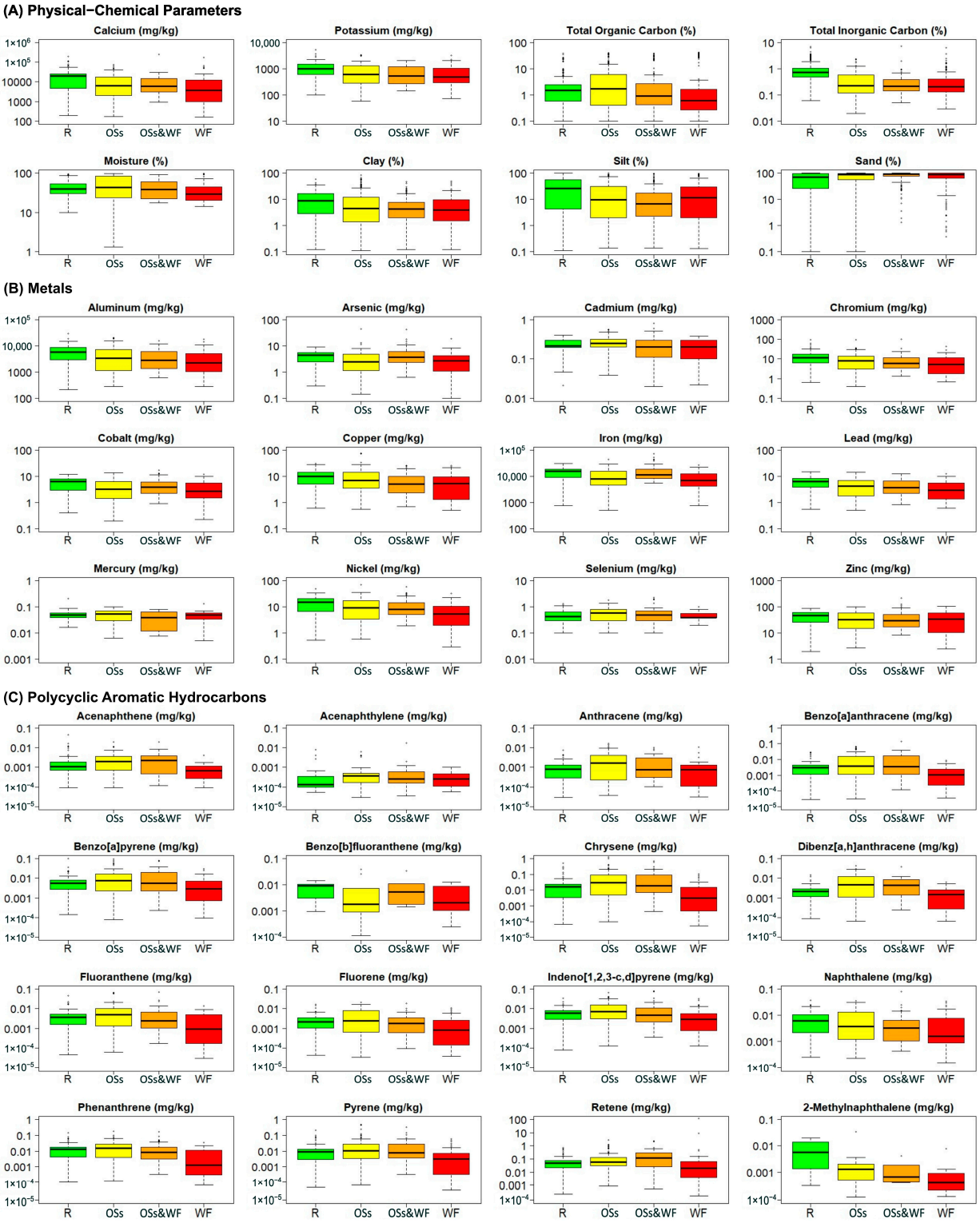


Figure 3. Box plots showing the distribution of physical–chemical parameters, metals, and PAHs for sediment samples, categorized by site classification (R = reference, OSs = oil sands, OSs&WF = oil sands and wildfire, and WF = wildfire). The central line indicates the median, the box represents the interquartile range, and the whiskers extend to values within 1.5 times the interquartile range. Outliers are shown as data points outside this range. The *y*-axis is on a logarithmic scale.

The wildfire-impacted sites exhibited significant decreases in the median concentrations of several metals in sediment samples, with all analyzed metals showing lower levels compared to the reference sites (Figure 3B; Table S4). The most substantial declines were observed for chromium, cobalt, copper, lead, nickel, and zinc. For example, chromium concentrations at both the WF and OSs&WF sites were more than 2 times lower than at the R sites, and zinc concentrations were approximately 1.2 times smaller at the wildfire-impacted sites compared to the R sites. The sharp reductions in these metals suggest that wildfire events may have altered sediment composition, potentially due to the removal of finer, metal-rich particles through erosion or the reduced deposition of metal-containing organic matter from burned landscapes. As highlighted in other research, wildfires are often associated with increased erosion and changes in the transport of metals from the soil zone, potentially leading to significant changes in metal concentrations in the soil zone [21,79]. The decrease in outlier frequency for most metals compared to water samples further reinforces the idea that post-wildfire conditions have led to a more uniform and depleted metal profile in sediments.

The concentrations of PAHs in sediment samples also showed a significant decline at wildfire-affected sites compared to reference locations (Figure 3C; Table S4). The most pronounced reductions were observed for chrysene, pyrene, fluoranthene, and benzo[a]anthracene, with their median values at both the WF and OSs&WF sites being up to 6 times lower than at the R sites. For example, chrysene concentrations at the WF sites were more than 5 times lower than at the R sites, and pyrene levels were approximately 3 times lower. Similarly, retene, a PAH commonly linked to wildfire combustion, showed fluctuating concentrations but ultimately exhibited a downward trend at both the WF and OSs&WF sites. The overall reduction in PAH levels, coupled with the decrease in the frequency of upper outliers, suggests that the wildfire event influenced sediment concentrations, leading to lower levels at wildfire-impacted sites. Studies have indicated that wildfires can result in a temporary increase in PAHs in both water and sediment [21,80], but changes in runoff and erosion processes can also lower these contaminant levels in sediments over time [81].

3.3. Temporal Water and Sediment Quality Variability in Wildfire-Affected Sites

The responses observed for water and sediment samples following wildfire events were generally opposite in nature, with increases in dissolved metals and PAHs in water samples, while sediment samples exhibited initial increases but long-term decreases in most of these compounds over time (Figures 4 and 5; Tables S5 and S6). To better understand the source, transport, and fate of these contaminants, box plots were generated to visualize parameter distributions at various time points: before the fire, during the fire, one year after (A1), two years after (A2), and three or more years after the fire (A3+). These visualizations provide insight into the temporal variability in compound concentrations and highlight the contrasting trends between water and sediment in wildfire-impacted areas.

In surface water samples, significant temporal variations were observed for multiple physical–chemical parameters, metals, and PAHs, following patterns reported in previous studies (Figure 4A–C; Table S5; [19,21,38]). Immediately after the fire, notable increases occurred in the median concentrations of several parameters, including phosphorus, TSSs, and turbidity. Additionally, elevated levels of metals such as aluminum, cobalt, and lead were detected within one to two years post-fire. For instance, phosphorus median concentrations were 1.1 times higher during the fire compared to pre-fire levels, while TSSs and turbidity increased by 1.1 and 1.4 times, respectively. These results indicate measurable post-fire increases in several water quality parameters. These observed patterns are consistent with the enhanced mobilization of fine sediments and associated contaminants,

potentially linked to increased runoff and erosion following wildfires. PAH concentrations also exhibited a distinct temporal pattern, with compounds such as retene, pyrene, and fluoranthene increasing significantly during and up to two years after the wildfire. Retene, a well-known biomarker of wildfire combustion, more than doubled in concentration during the wildfire and remained elevated for 2+ years. Despite these increases, PAH concentrations remained below established guidelines, indicating that while wildfires can cause substantial short-term impacts, long-term effects (beyond three years) were less evident in this dataset and may reflect reduced runoff and natural attenuation processes.

In contrast, sediment samples exhibited different temporal patterns, particularly in the years following the wildfire (Figure 5A–C; Table S6). While several metals and PAHs showed short-term increases immediately after the wildfire, their concentrations declined as early as one-year post-fire. For example, aluminum and lead concentrations were elevated immediately following the fire but gradually decreased over subsequent years. Similarly, PAH concentrations in sediments followed a comparable trend, with a marked decline after the initial post-fire period. This pattern suggests that although wildfires contribute to short-term increases in metals and PAHs in sediments, these compounds appear to be less persistent over time, likely due to increased erosion and the burial of surface contaminants. Increased erosion and the transport of metals and PAHs following wildfires have also been documented in previous studies [17,38,77,78]. Changes in sediment composition also reflected these shifts, with an initial increase in finer particles, such as clay and silt, while sand content decreased. This suggests that post-fire erosion processes play a key role in redistributing contaminants, leading to their transport to rivers and lakes.

The contrasting trends between water and sediment quality samples underscore the complexity of wildfire impacts on aquatic ecosystems. While water quality is immediately affected by elevated concentrations of metals and PAHs due to increased runoff and erosion, these contaminants are gradually diluted, settled, or removed through natural attenuation processes. In contrast, sediments initially act as a temporary sink for wildfire-derived contaminants, accumulating metals and PAHs in the short term. However, long-term trends indicate a decline in sediment concentrations, likely due to continuous erosion, resuspension, and deposition processes that redistribute these compounds downstream. The observed decrease in sediment contamination over time suggests that, although wildfires introduce a substantial influx of pollutants into aquatic environments, natural hydrodynamic and geochemical processes contribute to their eventual dispersal and burial. These findings highlight the importance of long-term monitoring of both water and sediment compartments to fully understand wildfire-driven contaminant fate and transport. Additionally, they emphasize the need for targeted monitoring strategies to mitigate immediate post-fire water quality degradation and address potential sediment-associated contaminant risks in affected watersheds.

3.4. Contaminant Transport Model: Water vs. Sediment

Based on the responses observed in both water and sediment quality data, increased runoff and erosion are interpreted as likely important mechanisms influencing the transport of contaminants. The rise in metals and PAHs in water samples, alongside the long-term decrease of these compounds in sediment samples, is consistent with an interpretation in which contaminants are mobilized from the soil into rivers during and after the wildfire event. In this study, water chemistry data provided evidence of temporal changes in dissolved and particulate-associated contaminants, while sediment data helped identify longer-term shifts in depositional conditions and contaminant storage. PAH patterns further supported wildfire-related inputs, and the sonde data provided higher-frequency observations of short-term water quality responses during wildfire events. Together, these

datasets support an integrated interpretation of contaminant transport and fate across environmental compartments. Figures 4 and 5 support this interpretation, showing clear temporal trends in both water and sediment quality that align with the expected effects of increased runoff. While PAHs are indeed produced during wildfires, they likely do not remain in the soil for long due to erosion and runoff, which transport them into river systems. This dynamic is further reinforced by the observed decrease in clay and silt content at sediment monitoring locations affected by wildfires, supporting the hypothesis of increased erosion in these areas.

These findings align with previous studies that have documented similar trends in wildfire-impacted areas [12,15,50–52], further supporting this interpretation of contaminant transport and fate. However, it is important to acknowledge that this study was conducted at a regional scale, and data may be diluted due to the broad spatial and temporal scope of the analysis. Despite these challenges, the overall trends remain consistent with findings from more localized studies, strengthening the interpretation of wildfire effects across a larger geographical area.

Additionally, monitoring locations affected by both industrial activities and wildfires exhibited the most pronounced impacts, consistent with data indicating that wildfire occurrence can exacerbate erosion in these locations. Increased erosion may facilitate the mobilization of PAHs and metals from the soil that would otherwise remain in place, allowing these contaminants to enter rivers and lakes more readily. These patterns are consistent with an important influence of wildfires on sediment and water quality. While the impact on water quality appears to diminish over time, with contaminant levels returning closer to baseline after approximately three years, the effects on sediment quality persist. Even after three years, sediment samples continue to show evidence of wildfire-related contamination, suggesting that the long-term effects on soils may be more enduring than those on water quality.

The conceptual model below illustrates the transport of PAHs and metals, which increase in the immediate aftermath of a wildfire and are subsequently transported to rivers via runoff and erosion. This model is intended as a synthesis of the patterns observed across the different datasets and summarizes the inferred sources, transport pathways, and likely fate of these contaminants over time (Figure 6). It is important to note that while these regional trends were observed, site-specific factors may lead to variations in response, underscoring the complexity of wildfire impacts on both water and sediment quality. Hence, the observed patterns in this investigation suggest that distinguishing between wildfire and industrial contributions is crucial, as their combined presence leads to more pronounced contamination signals. Box plots of water and sediment quality monitoring locations indicate greater variability in both metal and PAH concentrations when wildfires and industrial activities co-occurred. This underscores the need to clearly separate wildfire-derived and anthropogenic sources to better assess their individual and combined impacts, which will be explored in the following section.

3.5. Differentiating Wildfire vs. Industrial Impacts

Within the region of investigation, wildfires and oil sands activities represent the two primary sources of PAHs in the environment. The RAMP and LTRN datasets were analyzed for these source apportionments through the following techniques.



Figure 4. Box plots showing the distribution of physical–chemical parameters, metals, and PAHs for water samples from wildfire-affected sites, categorized by temporal variation: before (B), during (D), one year after (A1), two years after (A2), and three or more years after the fire (A3+). The central line indicates the median, the box represents the interquartile range, and the whiskers extend to values within 1.5 times the interquartile range. Outliers are shown as data points outside this range. The *y*-axis is on a logarithmic scale, and PAH guideline values are indicated by the red dashed line (when available).

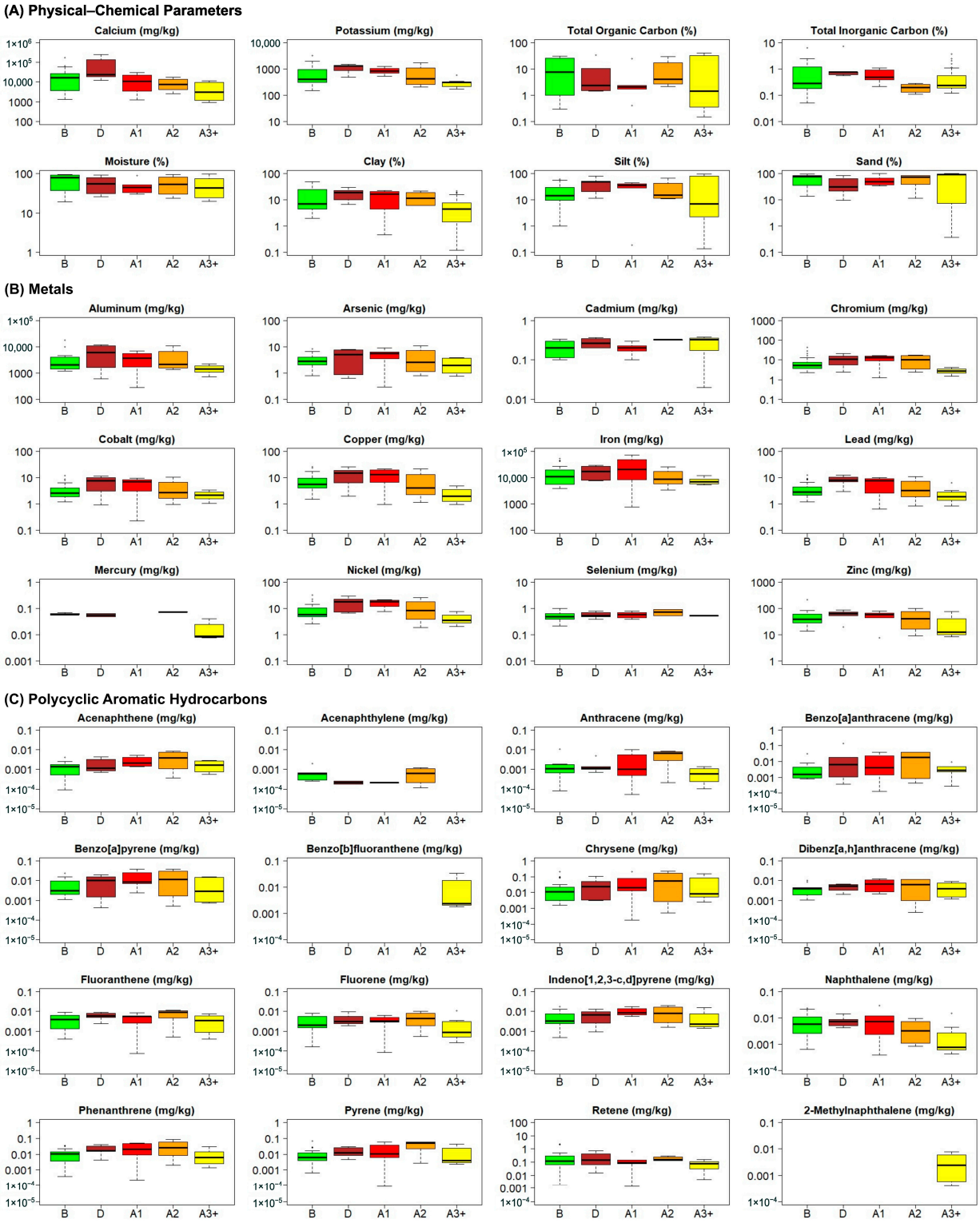


Figure 5. Box plots showing the distribution of physical–chemical parameters, metals, and PAHs for sediment samples from wildfire-affected sites, categorized by temporal variation: before (B), during (D), one year after (A1), two years after (A2), and three or more years after the fire (A3+). The central line indicates the median, the box represents the interquartile range, and the whiskers extend to values within 1.5 times the interquartile range. Outliers are shown as data points outside this range. The *y*-axis is on a logarithmic scale.

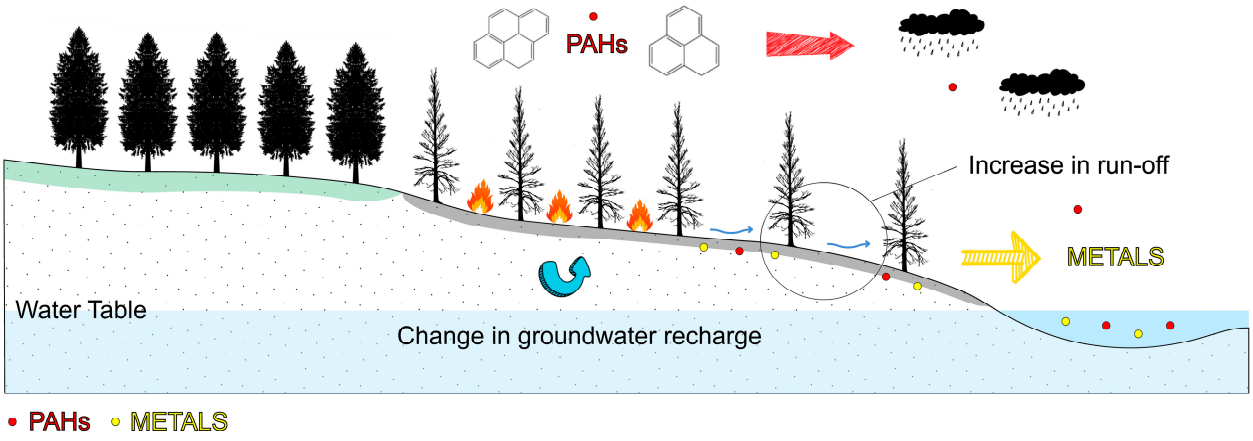


Figure 6. A conceptual model synthesizing observed patterns and inferred pathways for the transport and fate of polycyclic aromatic hydrocarbons (PAHs) and metals in water and sediment following a wildfire. Blue arrows represent run-off and groundwater recharge, red arrows represent transport of PAHs, and yellow arrows represent mobilization of metals.

3.5.1. Relative Concentrations of Parent Versus Alkylated PAHs

The ratios of parent and alkylated PAHs were determined relative to the total PAHs present in the water and sediment samples, based on both the spatial (Figure 7; Tables S8 and S9) and temporal characterization (Figure 8; Tables S10 and S11). Elevated temperatures associated with the wildfire promote thermal degradation of alkyl side chains, resulting in a lower relative abundance of alkylated compounds compared to parent PAHs [44,51]. Consequently, spatial and site characterization could show a higher relative concentration of parent PAHs in both the water and sediment matrices at sites exclusively impacted by wildfire (WF), compared to sites influenced by oil sands (OSs) or a combination of oil sands and wildfire (OSs and WF). This trend was more pronounced in the sediments phase, where the WF sites exhibited median parent-to-total PAHs ratios 1.46 to 2.22 times higher than those sites impacted by OSs and OSs&WF, respectively. In the water phase, the median parent-to-total PAHs ratios were found to be 1.48 to 1.83 times greater than those observed at sites impacted by OSs and OSs&WF, respectively. Median parent-to-total PAHs ratios at the WF sites were comparable to those at the reference sites, likely a result of the cumulative data from multiple wildfire-impacted sites with burn histories spanning several weeks to multiple months prior to sampling.

Temporal trends in parent and alkylated PAHs in the water matrix showed a decline in the median values immediately following the fire, followed by a gradual increase in subsequent years. Based on the observations described in Section 3.3, median values of parent PAHs in the sediment matrix were expected to show a slight increase immediately after the fire, followed by a decline in the years thereafter. However, the median values of the alkylated PAHs in the sediment matrix remained relatively stable during and after the fire period. The absence of a pronounced increase in parent PAHs relative to alkylated PAHs can be attributed to the elevated concentrations of certain alkylated PAHs that are also associated with wildfire inputs, including retene, 1-methylnaphthalene, 2-methylnaphthalene, 2-methyl-phenanthrene, and 2-methyl-anthracene [48]. In addition, volatilization of some PAHs during combustion may further influence the relative proportions of parent and alkylated PAHs [48,82]. Collectively, these observations indicate that these bulk comparisons of parent and alkylated PAHs alone are insufficient to reliably distinguish between pyrogenic and petrogenic PAH sources.

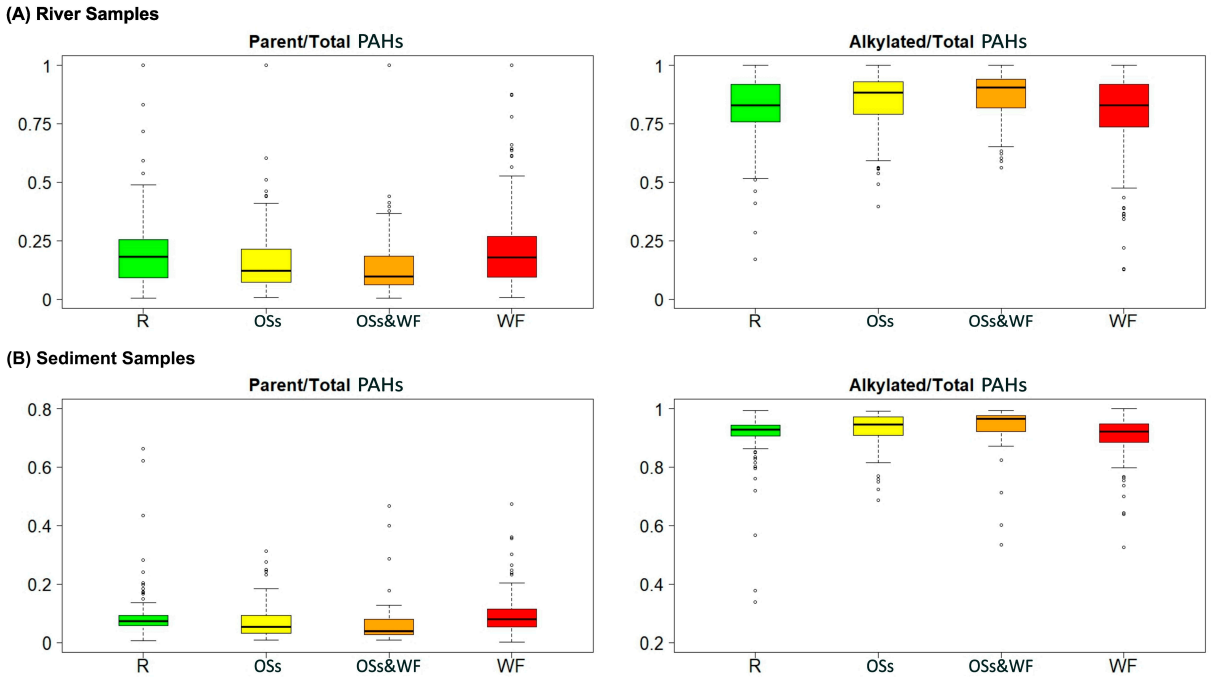


Figure 7. Box plots showing the distribution of the ratio of parent/total PAHs and alkylated/total PAHs for (**A**) river and (**B**) sediment samples, categorized by site classification (R = reference, OSs = oil sands, OSs&WF = oil sands and wildfire, and WF = wildfire). The central line indicates the median, the box represents the interquartile range, and the whiskers extend to values within 1.5 times the interquartile range. Outliers are shown as data points outside this range.

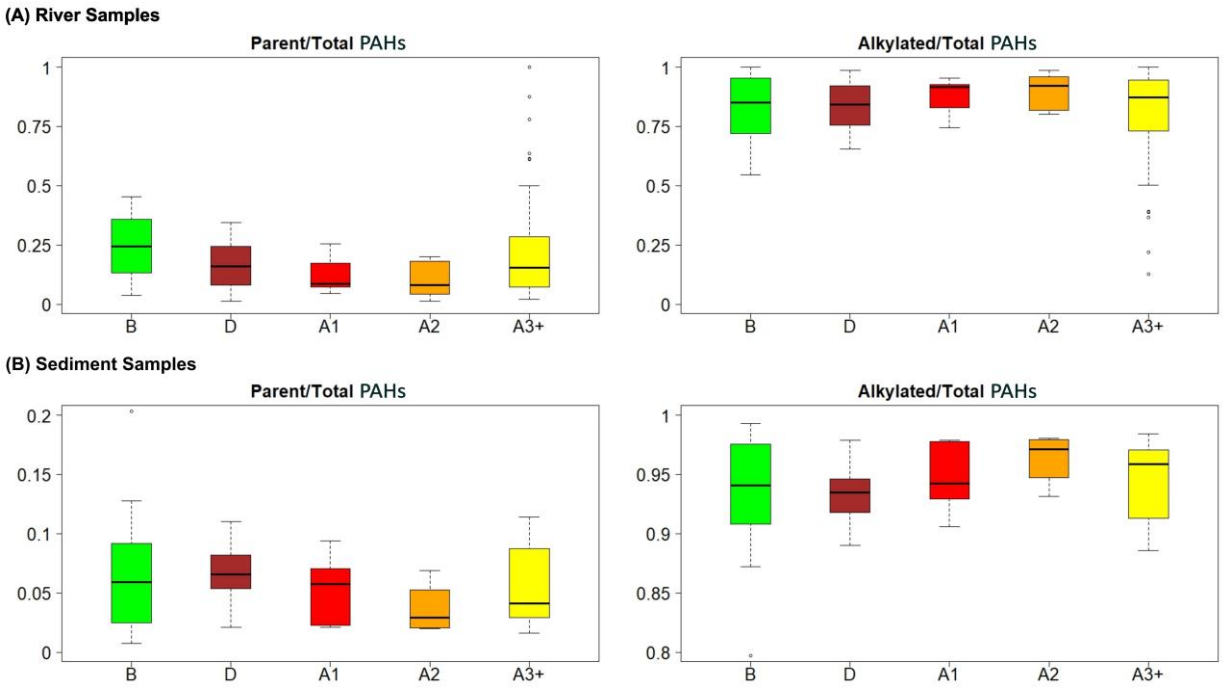


Figure 8. Box plots showing the distribution of the ratio of parent/total PAHs and alkylated/total PAHs for (**A**) river and (**B**) sediment samples from the wildfire-affected sites, categorized by temporal variation: before (B), during (D), one year after (A1), two years after (A2), and three or more years after the fire (A3+). The central line indicates the median, the box represents the interquartile range, and the whiskers extend to values within 1.5 times the interquartile range. Outliers are shown as data points outside this range.

3.5.2. Diagnostic Ratios

i. Pyrogenic Index

The pyrogenic index (PI) was calculated for the river and sediment samples for both the spatial characterization (Figure 9; Tables S8 and S9) and temporal characterization (Figure 10; Tables S10 and S11) datasets. Reported PI values typically range from 0.8 to 2 for pyrogenic sources, with substantially lower values associated with petrogenic inputs, including <0.01 for crude oils and <0.05 for heavy oils [51,53,54]. Elevated temperatures associated with pyrogenic processes promote thermal degradation of alkyl side chains, resulting in a higher relative abundance of parent PAHs, and consequently, higher PI values. In contrast, the extensive alkylation produced during low-temperature thermogenic processes over a geological time scale leads to lower PI values for petrogenic PAHs.

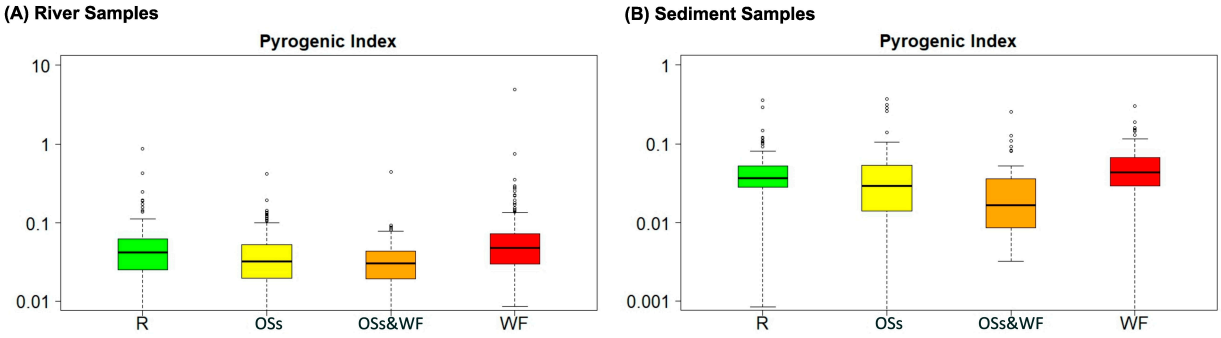


Figure 9. Box plots showing the distribution of the pyrogenic ratios for (**A**) river and (**B**) sediment samples, categorized by site classification (R = reference, OSs = oil sands, OSs&WF = oil sands and wildfire, and WF = wildfire). The central line indicates the median, the box represents the interquartile range, and the whiskers extend to values within 1.5 times the interquartile range. Outliers are shown as data points outside this range.

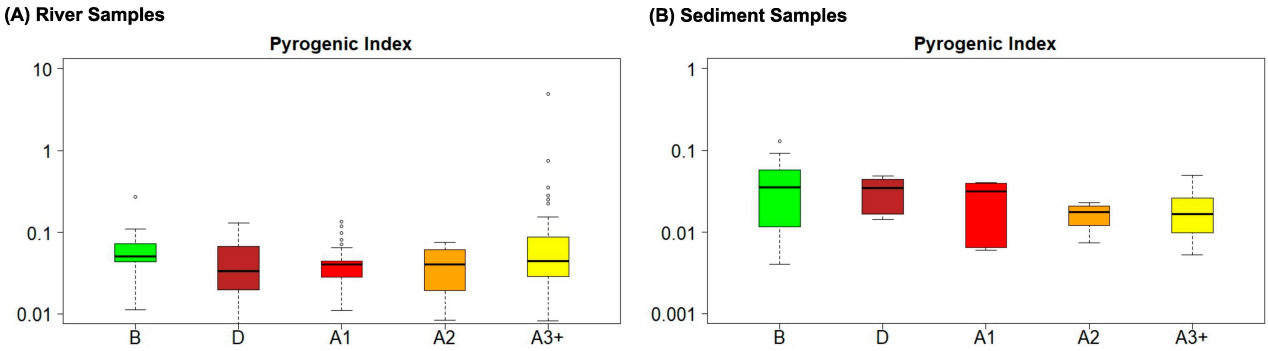


Figure 10. Box plots showing the distribution of the pyrogenic ratios for (**A**) river and (**B**) sediment samples from the wildfire-affected sites, categorized by temporal variation: before (B), during (D), one year after (A1), two years after (A2), and three or more years after the fire (A3+). The central line indicates the median, the box represents the interquartile range, and the whiskers extend to values within 1.5 times the interquartile range. Outliers are shown as data points outside this range.

These expected trends were observed in both the water and sediment phases within the spatial characterization dataset. The median PI values at the WF-impacted sites were 1.49 to 1.6 times higher than those at sites impacted by OSs and OSs&WF, respectively. This response was more pronounced in the sediment matrix, where the median PI values at the WF sites were 1.47 to 2.62 times higher than those observed at the OSs and OSs&WF, respectively (Figure 9). Consistent with the trends observed for the relative proportions of parent and alkylated PAHs, the PI values did not exhibit any clear temporal patterns and

could not independently differentiate between pyrogenic and petrogenic PAHs sources within the temporal dataset (Figure 10).

ii. PAH Ratios

In this study, diagnostic PAHs ratios, including of fluoranthene/(fluoranthene + pyrene) [Fla/(Fla + Pyr)], retene/(retene + chrysene) [Ret/(Ret + Chy)], and cross-plot of benzo(a)anthracene/(benzo(a)anthracene + chrysene) versus fluoranthene/(fluoranthene + pyrene) [BaA/(BaA + Chy) vs. Fla/(Fla + Pyr)] were used to distinguish between petrogenic and pyrogenic PAH sources (Figures 11 and 12). The application of these ratios for source apportionment is well supported in the literature [83,84]. Fla/(Fla + Pyr) values below 0.4 are typically associated with a petrogenic source, values between 0.4–0.5 with petroleum combustion, and values greater than 0.5 with a coal or softwood combustion source (Figure 11) [83,84]. Similarly, Ret/(Ret + Chy) values between 0.15–0.50 are indicative of petroleum combustion, values between 0.30–0.45 correspond to coal combustion, and values between 0.83–0.96 are characteristic of softwood combustion sources (Figure 11) [83,84].

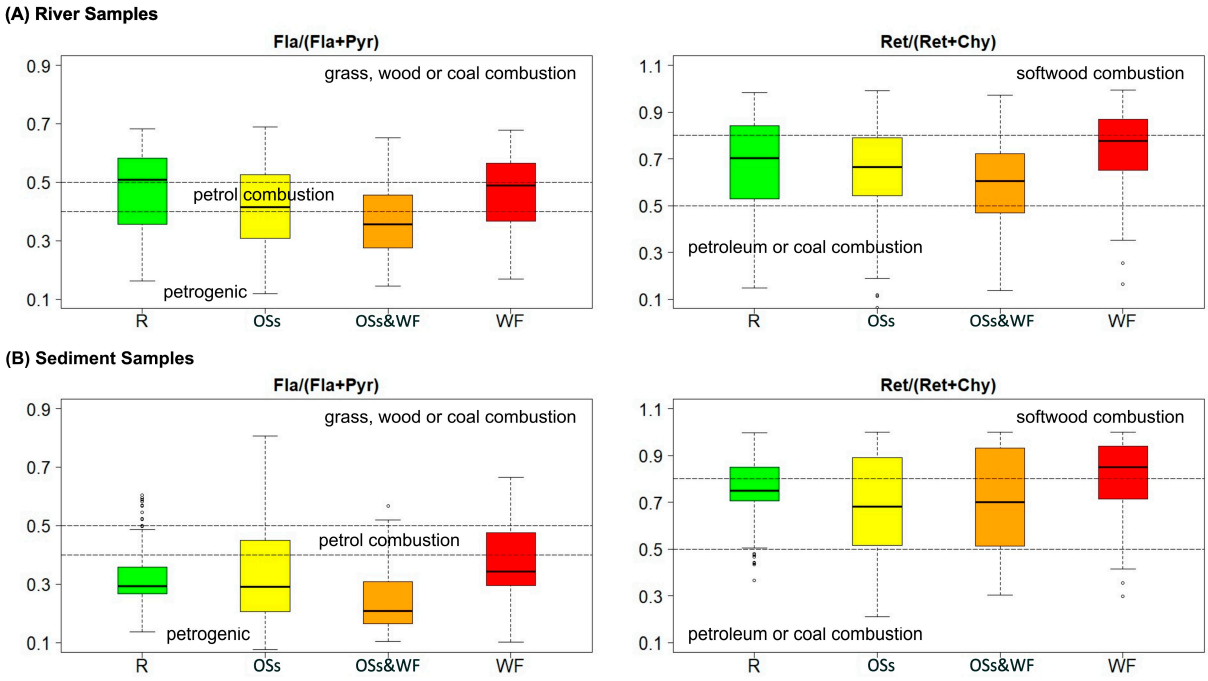


Figure 11. Box plots showing the diagnostic ratios of fluoranthene/(fluoranthene + pyrene) and retene/(retene + chrysene) for (**A**) river and (**B**) sediment samples, categorized by site classification (R = reference, OSs = oil sands, OSs&WF = oil sands and wildfire, and WF = wildfire). The central line indicates the median, the box represents the interquartile range, and the whiskers extend to values within 1.5 times the interquartile range. Outliers are shown as data points outside this range. Dashed horizontal lines indicate the reference threshold values for interpreting the diagnostic ratios and distinguishing among potential PAH sources.

In the water matrix, both Fla/(Fla + Pyr) and Ret/(Ret + Chy) ratios were higher at the WF-impacted sites compared to the sites influenced by OSs and OSs&WF, with median values ranging from 1.2 to 1.4 times higher (Figure 11; Table S8). This effect was more pronounced in the sediment matrix, where the median values at the WF-impacted sites were 1.2 to 1.7 times higher than those observed at the OSs and OSs&WF sites (Table S9). The response of Fla/(Fla + Pyr) ratios at the WF-impacted sites was generally similar to that observed at reference sites, indicating no clear wildfire-specific signal. In contrast, Ret/(Ret + Chy) ratios exhibited a more distinct response relative to reference conditions,

with median values approximately 1.1 times higher at wildfire sites, further supporting the utility of retene as a biomarker of wildfire influence [48]. The temporal trends in the diagnostic PAH ratios generally mirrored those observed for individual PAH compounds (Section 3.3), with increasing ratios in the water matrix following wildfire events and initial post-fire increases, followed by long-term decline in the sediment matrix (Figure 12; Tables S10 and S11).

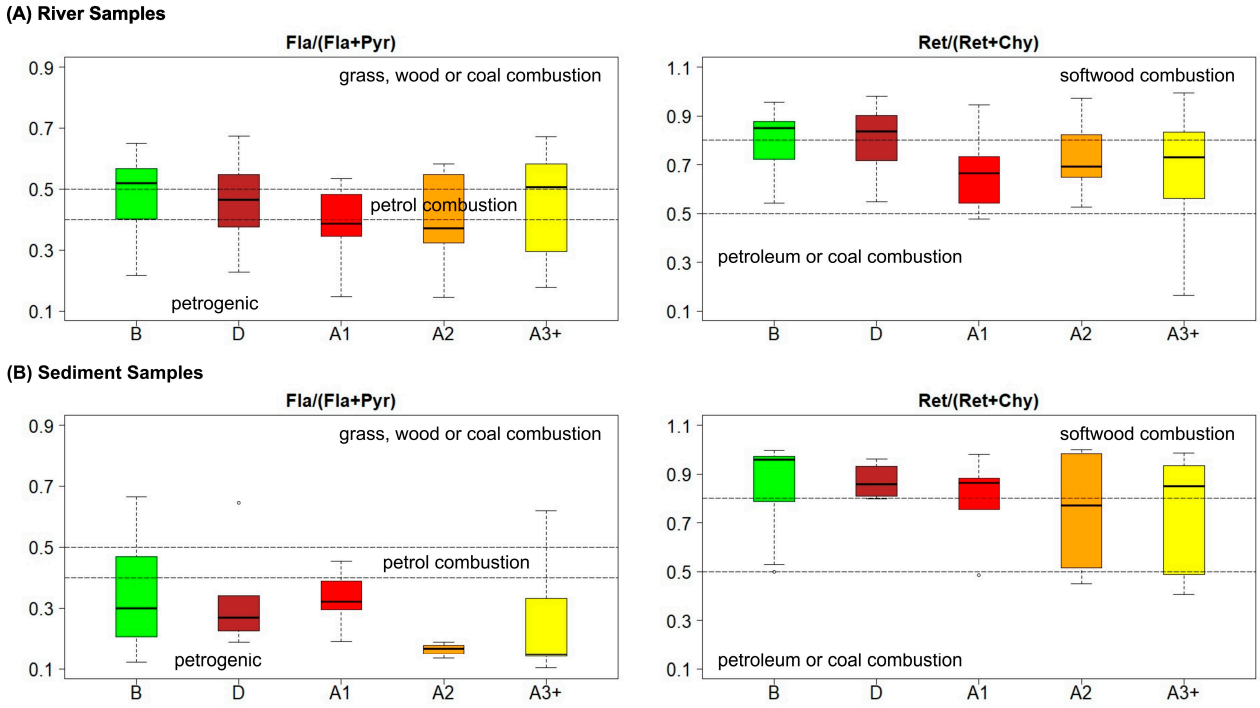


Figure 12. Box plots showing the diagnostic ratios of fluoranthene/(fluoranthene + pyrene) and retene/(retene + chrysene) for (**A**) river and (**B**) sediment samples from the wildfire-affected sites, categorized by temporal variation: before (B), during (D), one year after (A1), two years after (A2), and three or more years after the fire (A3+). The central line indicates the median, the box represents the interquartile range, and the whiskers extend to values within 1.5 times the interquartile range. Outliers are shown as data points outside this range. Dashed horizontal lines indicate the reference threshold values for interpreting the diagnostic ratios and distinguishing among potential PAH sources.

iii. PAH Cross-plots

The bivariate relationship between benzo(a)anthracene/(benzo(a)anthracene + chrysene) versus fluoranthene/(fluoranthene + pyrene) [BaA/(BaA + Chy) vs. Fla/(Fla + Pyr)] has been widely applied to differentiate between petrogenic and pyrogenic sources, including petroleum contamination and petroleum combustion versus wood combustion [83,85,86]. In this study, all water and sediment samples were plotted on the BaA/(BaA + Chy) vs. Fla/(Fla + Pyr) cross-plot (Figure 13). The reference (R), oil sands (OSs), oil sands and wildfire (OSs&WF), and wildfire (WF) sites were distributed across the three source domains, with no clear separation among site categories.

This lack of clear clustering may be attributed to the broad spatial and temporal scope of the dataset, which reduced the discriminatory power of this diagnostic approach in the present application. The dataset integrates samples collected from the wildfire-impacted sites spanning monitoring intervals, ranging from several weeks to multiple years, meaning that immediate short-term post-fire responses may not have been consistently captured. As a result, pyrogenic signatures associated with wildfire inputs may have been progressively

missed and attenuated over time, and further reduced by dilution effects, leading to the diffused and overlapping distribution of data points observed in Figure 13.

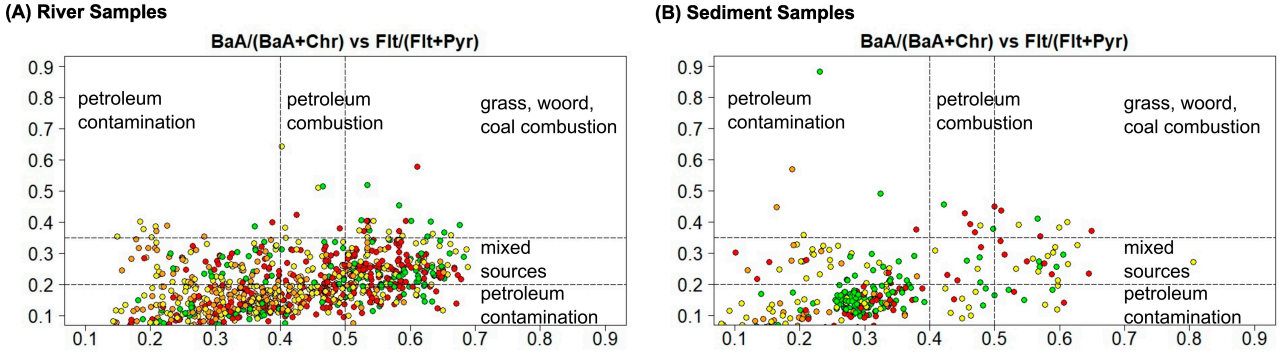


Figure 13. Scatter plots showing the diagnostic ratios of benzo(a)anthracene/(benzo(a)anthracene + chrysene) versus fluoranthene/(fluoranthene + pyrene) for (**A**) river and (**B**) sediment samples, categorized by site classification. Green, yellow, orange, and red circles represent reference (R), oil sands (OSs), oil sands and wildfire (OSs & WF), and wildfire (WF) sites, respectively.

Based on these findings, effective differentiation between pyrogenic (wildfire-derived) versus petrogenic (oil sands-derived) PAH sources requires the combined application of multiple diagnostic ratios rather than reliance on a single ratio or cross-plot [44,48–51,53–56]. Furthermore, concurrent sampling of both the sediment and water matrices is essential for understanding the transport and fate of PAHs in the aquatic environment. PAHs preferentially adsorb onto suspended sediments, where they can persist for extended periods in the particulate form. As these contaminated particulates are transported through the watershed, PAHs may re-partition into the dissolved phase, thereby influencing surface water quality, as well as hydraulically connected groundwater systems downstream of the burned area [87–89].

3.6. Hydrological Impacts of Wildfires

3.6.1. Model Performance, Parameter Transferability, and Forcing Sensitivity

Domain-wide calibration on the working ~3 km grid produced stable performance after screening resolved drainage-area inconsistencies and GRU mask issues. KGE improved while volumetric error trends flattened (Figure S3) with increasing class fraction, indicating physically coherent behaviour at scale and consistent routing once map corrections were applied. These outcomes followed the staged DDS optimization described in the Methods Section (coarse screening → production calibration → sub-domain refinement → consolidated run) and were corroborated using WSC hydrograph evaluations, where local misfits diminished downstream as expected for a transferable parameter set. The final configuration used a single consolidated parameterization across 2015–2022 that preserves class-based physical meaning, with only minor localized adjustments where lake or channel influences required them.

GRU-linked runoff generation parameters demonstrated strong transferability across basins (Table S12), which is essential for wildfire attribution in this study because it ensures that scenario differences arise from land-cover change rather than parameter drift. Parameters optimized in the Clearwater River (dominated by the mapped "grass"/early-successional cover) transferred effectively to the Christina River with only light routing tweaks, whereas the Muskeg–Steepbank sub-domain required targeted refinement of recharge and snowmelt terms for wetland-rich and conifer/mixedwood classes due to stronger storage and cold-season controls (Table S12). The Athabasca mainstem, which lacks full upstream coverage in the model domain, was retained primarily for timing

diagnostics rather than mass–balance evaluation; this pragmatic treatment maintained routing continuity without confounding the class-based calibration.

Hydrometeorological forcing sensitivity was the dominant external uncertainty relevant to wildfire impact magnitude. Calibrations driven by RDPA–CaPA precipitation with RDPS one-day-ahead temperature produced consistent behaviour across the domain and served as the baseline for scenario work, while comparative tests with RDRS yielded substantially higher simulated volumes in independent basins (e.g., Black River and Firebag River over 2015–2018), underscoring that forcing choice can inflate or dampen post-fire runoff signals. Ongoing attrition of conventional ECCC climate stations within the RAMP domain, where more than a dozen long-record stations operating between 1980 and 2022 have declined to only three remaining in recent years, further reduces confidence in capturing short-duration, high-intensity precipitation events, meaning that some high peaks and high-volume events are likely missed simply because no station recorded them. Consequently, even gridded forcing products, such as RDRS, inherit this observational gap, and wildfire scenario envelopes must therefore be interpreted in parallel with forcing-ensemble sensitivity to reflect this growing data-sparsity-driven uncertainty.

3.6.2. Wildfire Effects on Runoff Partitioning and Watershed-Scale Hydrologic Response

Runoff increased following wildfire, with post-fire configurations producing consistently larger storm-integrated responses than the pre-fire baseline (Figure 14). Although only the Clearwater, Christina, and Steepbank rivers mainly experienced wildfire disturbance—and the burned portions of these basins represent relatively small fractions of their total gauged areas (Figure S1D)—the 8-year hydrograph volumes still show an increase in basin-integrated runoff. Using the mean annual precipitation of ~500 mm and the pre-fire runoff of ~150 mm, the post-fire period yields an additional ~80 mm of runoff over eight years (approximately ~10 mm yr^{-1}), where about 30% of the watershed area was burned. Against this quantitative backdrop, the modelled hydrographs (Figure 15) also show clear qualitative differences: the post-fire traces separate from the baseline during rainfall and melt events, and post-fire configurations produce more pronounced responses during peak input periods, amounting to roughly a ten-percent increase in storm-integrated runoff under comparable forcing. Together, these results indicate that while only modest outlet-scale changes are expected in basins where the burned fraction is limited, wildfire still produces a detectable basin-integrated increase in runoff proportional to the extent of disturbance.

The Baseflow Index (BFI) maps demonstrate a coherent reorganization of runoff pathways from groundwater-dominated (slow-flow) to event-dominated (quick-flow) conditions following wildfire. In the pre-fire BFI map (Figure 16a), areas with a higher BFI identify stronger groundwater discharge zones and longer subsurface residence times, consistent with a hydrologic regime buffered by storage and sustained drainage. In the post-fire BFI map (Figure 16b), the BFI decreases are concentrated in burn-affected grids, signalling reduced recharge to and drainage from the saturated zone, along with a larger share of near-surface runoff reaching channels. The magnitude of the BFI decline covaries with the spatial footprint of regeneration and burn severity proxies, where canopy loss and soil surface alteration diminish interception and infiltration, shorten travel times, and increase the frequency and persistence of shallow flow paths. In contrast, wetlands and riparian complexes mute BFI changes by preserving local storage and hydraulic connection to the groundwater system. Together, Figure 16a,b indicate that wildfire shifts the pathway balance toward shallower, faster responses, aligning with the post-fire increase in storm-integrated runoff shown in Figure 14.

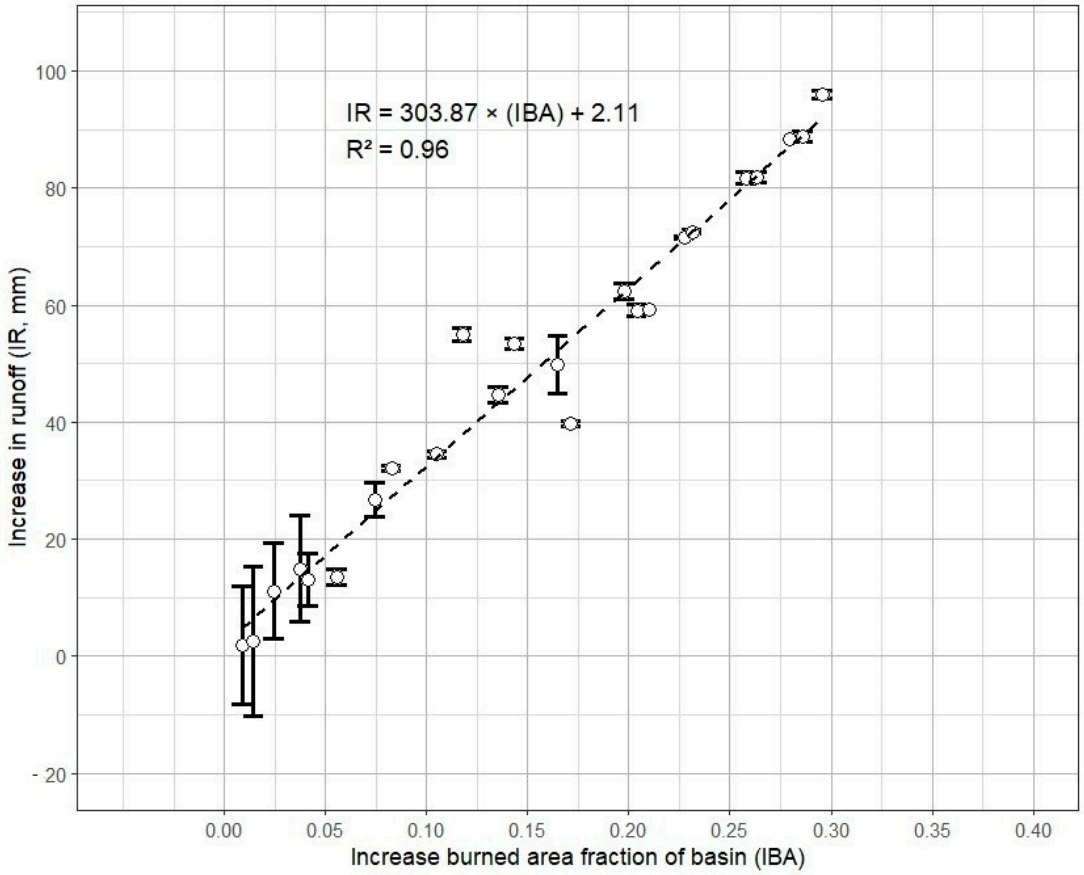


Figure 14. Relationship between burned area fraction and runoff increase (mean ± 1 SD).

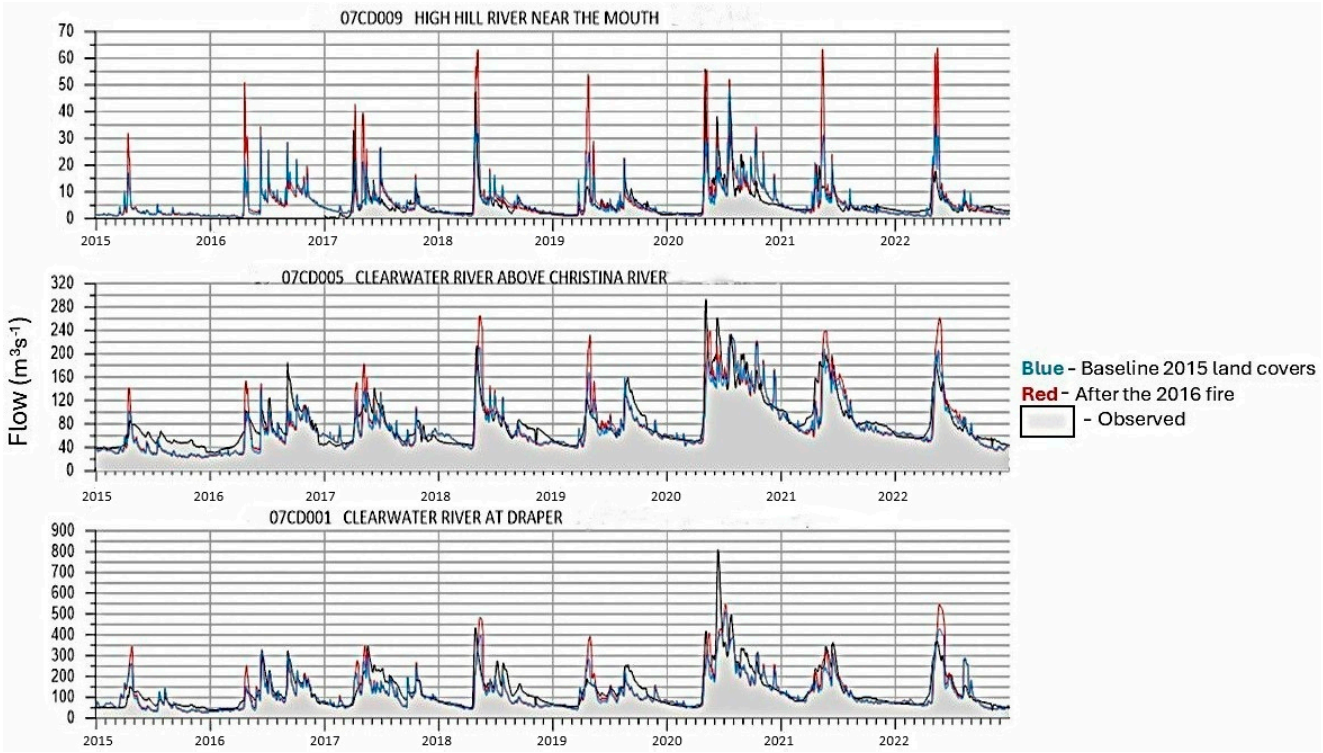
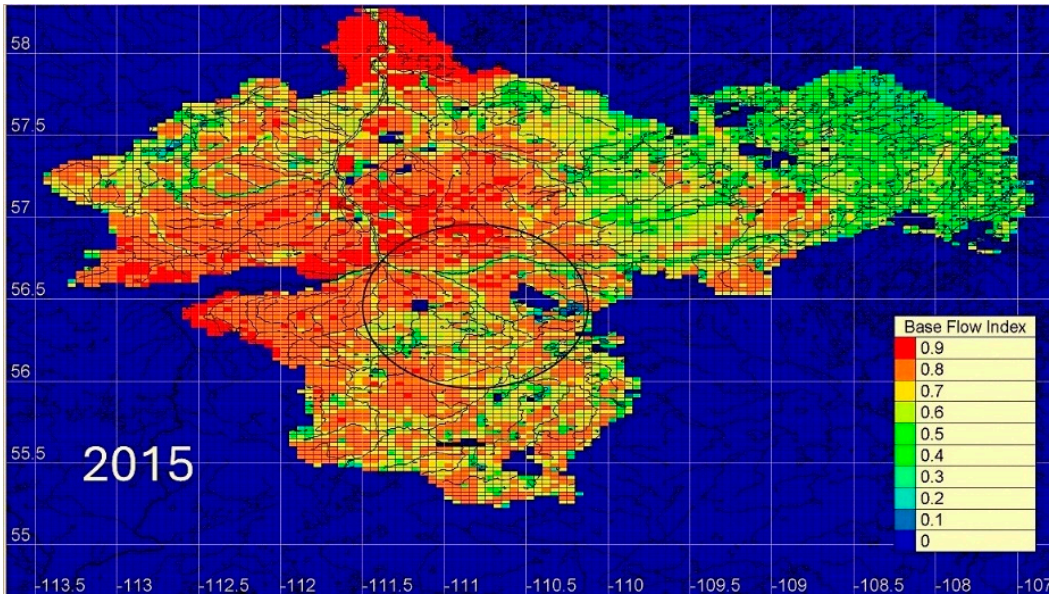
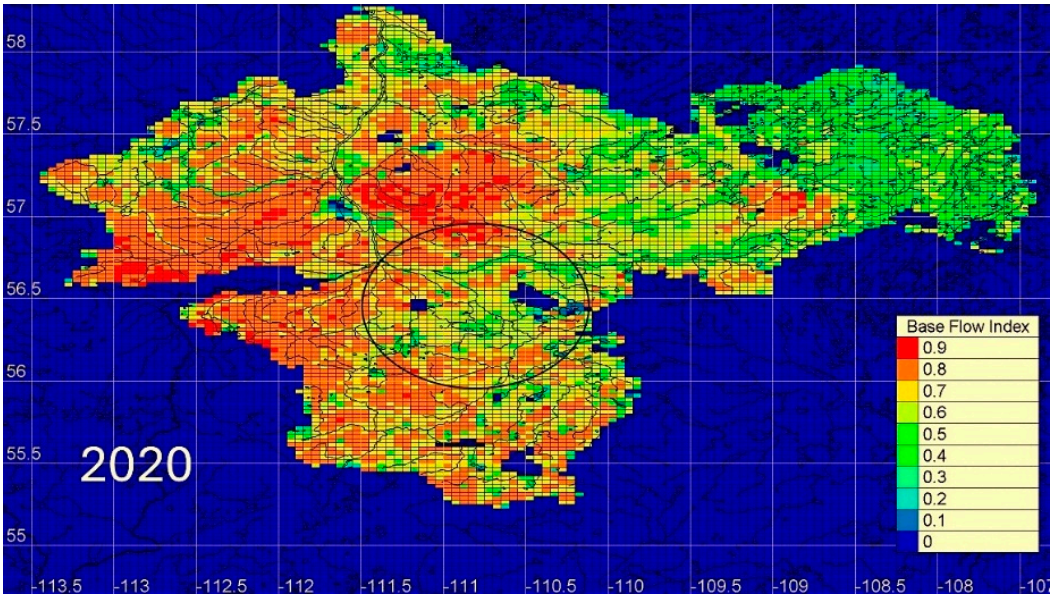


Figure 15. Hydrographs comparing baseline and post-fire response during representative events.



(**a**)



(**b**)

Figure 16. Spatial distribution of the BFI before (**a**) and after (**b**) wildfire, with the circled region indicating the approximate area affected by the 2016 Horse River ("The Beast") Fire.

The basin-integrated BFI time series corroborates these spatial patterns by revealing a systematic temporal reduction in baseflow contribution after the fire (Figure 17). During rainfall and melt events, the post-fire BFI trace diverges downward from the baseline, demonstrating that a smaller proportion of total flow is sourced from groundwater when the catchment is disturbed. The divergence is most pronounced during high-intensity precipitation and rapid melt episodes, when diminished infiltration and amplified near-surface connectivity expedite translation of inputs to channelized flow. Between events, BFI recovery is incomplete: although values rise as the system relaxes toward background conditions, they do not return to pre-fire levels over the observation window. This partial recovery implies persistent depletion or decoupling of subsurface storage, likely driven by a combination of altered soil structure, reduced macropore effectiveness, and ongoing vegetation recovery dynamics that maintain higher event efficiencies relative to the

baseline. The temporal signature, therefore, provides process-level evidence that wildfire reduces the slow-flow fraction while elevating the quick-flow share of the hydrograph, in agreement with the spatial redistribution of the BFI and the elevated event runoff volumes noted above.

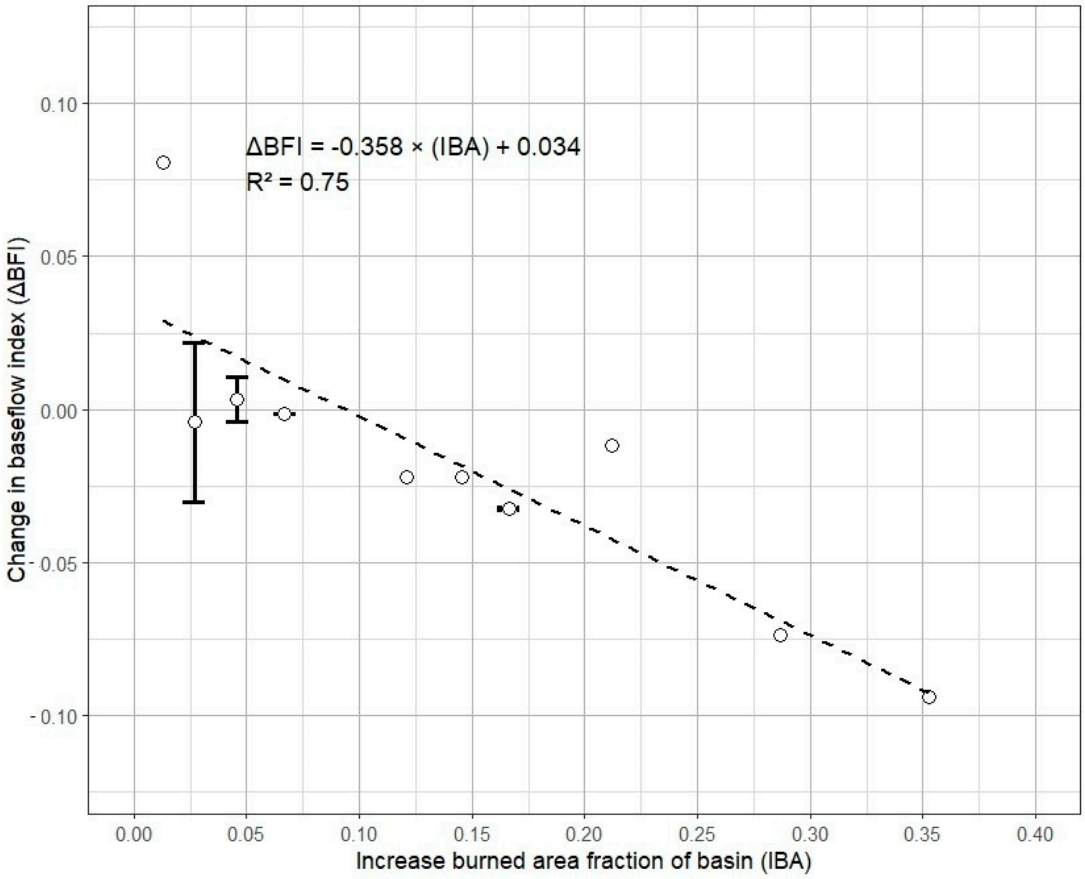


Figure 17. Change in baseflow index (BFI) as a function of burned area fraction (mean ± 1 SD).

Hydrographs (Figure 15) from representative events integrate these partitioning changes into the observable flow response at the outlet. Post-fire hydrographs exhibit steeper rising limbs and higher, sharper peaks than the baseline for comparable meteorological inputs, reproducing the combined effects of lower infiltration capacity, greater overland and near-surface connectivity, and shorter hillslope travel times. Recession segments are correspondingly curtailed, with more rapid declines toward low flow once inputs cease, reflecting reduced groundwater sustenance and diminished drainage from intermediate storage elements. The timing of peak occurrence is advanced relative to the baseline, and the post-fire hydrograph volume during events is larger, consistent with the approximate ten percent increase in storm-integrated runoff and the indicated reduction in infiltration after the burn. In turn, the attenuated recession supports the basin-integrated BFI evidence of a lasting reduction in slow-flow support between events. The concurrence of these features—greater event efficiency and peak magnitudes, accelerated response timing, and weaker recessions—demonstrates that wildfire reorganizes watershed function from a mixed groundwater–surface water regime toward one dominated by rapid, shallow pathways. This integrated behaviour is anticipated by the runoff comparison in Figure 14 and the spatial and temporal BFI responses in Figures 16 and 17, and is further supported by the observations of higher peaks (Figure 15).

Collectively, the four figures provide a consistent, mechanistic narrative of post-fire hydrologic transformation. The fire reduces infiltration capacity and deep percolation, increases the fraction of incident water routed along shallow pathways, and elevates event efficiency, which yields higher and faster peaks and a diminished contribution from groundwater during and after storms. The spatial localization of the BFI decline in burn-affected grids demonstrates that these changes are process-consistent and tied to the disturbance footprint, while the temporal BFI record and hydrographs show that the functional impacts persist beyond individual events and are evident at the watershed scale. In sum, wildfire shifts runoff partitioning from slow-flow dominance toward quick-flow dominance, and accelerates watershed-scale hydrologic response, producing larger, peakier events and weakened baseflow support in the post-fire regime

3.6.3. Implications for Wildfire Impact Attribution

The initial modelling experiments confirm that the WATFLOOD®/CHARM® framework is well-suited for attributing wildfire-driven hydrologic change across the RAMP domain. Consistent performance across multiple grid resolutions demonstrates that the consolidated parameter set is broadly transferable and can be applied at varying spatial scales without loss of fidelity. Paired scenario simulations show clear wildfire impacts: post-fire landscapes produced roughly 10% more total runoff, generated higher and more responsive peak flows, and exhibited reduced infiltration due to canopy loss, diminished interception, altered near-surface hydraulic properties, and the formation of hydrophobic soil layers that limit infiltration and enhance overland connectivity. These changes indicate a systematic shift in watershed flow partitioning toward surface and near-surface pathways, providing a mechanistic explanation for increased event flashiness and associated sediment and water quality responses. Collectively, these results establish a strong basis for domain-wide disturbance simulations and support the use of GRU-based distributed hydrologic modelling for wildfire impact assessment and cumulative-effects monitoring.

3.6.4. Limitations, Uncertainties, and Future Work

Several structural and data-related limitations were identified during model development. Anomalously high simulated stream flows in the Mackay and Muskeg rivers were traced to mis-specified wetland storage and conductivity parameters; correcting these resolved inflated runoff and underscored the model's sensitivity to wetland representation in flat, storage-rich terrain. The initial land-cover dataset also lacked burn and regeneration classes, limiting disturbance representation, which was addressed by constructing paired pre-fire and post-fire LULC layers; although WATFLOOD® can swap land-cover maps dynamically, new code may be needed to initialize classes that appear mid-simulation, whereas class removal is already supported. Grid construction introduced further uncertainty: several cells exhibited "frac = 0" due to latitude–longitude distortions and automated drainage-area assignment that followed lowest elevations rather than channels, requiring targeted correction to maintain coherent routing. Because the upper Athabasca basin lies outside the domain, upstream inflows cannot be simulated, but the mainstem was retained for routing continuity, with flows inserted only where gauges exist, which is sufficient at the 3 km working resolution. Finally, hydrometeorological uncertainty remains a key limitation: while RDPA–CaPA with RDPS produced stable calibrations, RDRS generated substantially larger volumes in independent basins, and declining ECCC station density across the domain reduces confidence in peak-flow depiction, particularly for short-duration convective rainfall.

As well, during the 8-year calibration period, regeneration of the fire-affected area was obviously occurring, so the calibration must be seen as an approximation—i.e., it is not a hydrological calibration for a point in time. However, even with this limitation, the distinction between the before and after fire modelling results is quite clear.

Future work will generate naturalized flow simulations to establish an undisturbed baseline against which landscape disturbances, especially wildfire, can be quantified across space and time. Building on this hydrologic foundation, we will extend the framework to post-fire sediment dynamics (e.g., adapting WATFLOOD® sediment/tracer capabilities) [90] and pathogen transport [91], enabling evaluation of how changes in vegetation, soil stability, hydrophobicity, and runoff pathways influence erosion, contaminant mobility, and water quality risk under increasing wildfire frequency and severity. These enhancements, together with continued refinement of burned and regenerating land-cover inputs and multi-forcing ensembles, will strengthen attribution and cumulative-effects assessment across the RAMP region.

3.7. Key Parameters for Monitoring Wildfire Impact

3.7.1. Continuous Monitoring of Physical Parameters

While the available data from the long-term monitoring network did not allow for a detailed evaluation of dissolved oxygen and pH responses, conductivity and turbidity emerged as key early indicators of wildfire activity. At the RIF monitoring location, shifts in conductivity and turbidity were detected shortly after the wildfire began, reflecting immediate changes in water quality likely linked to the wildfire (Figure 18). In contrast, at the HHR location, these changes took longer to appear, suggesting a delayed response in water quality impacts at this site (Figure 18). These differences highlight the spatial variability in wildfire effects and the need for both short- and long-term monitoring strategies to capture the full spectrum of wildfire impacts.

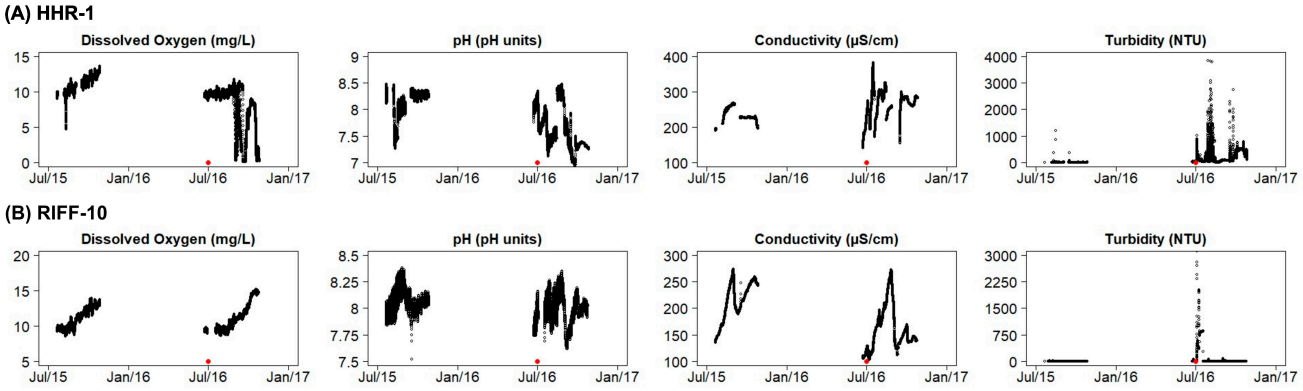


Figure 18. Time series of dissolved oxygen, pH, conductivity, and turbidity for two monitoring locations (HHR-1 and RIFF-10), with the red line indicating the date of the wildfire in the region.

These findings reinforce the value of continuous monitoring of key parameters, such as conductivity, turbidity, and dissolved oxygen. Previous studies have emphasized that continuous monitoring using water quality sondes can provide critical early indicators of wildfire-related impacts, allowing for a quicker response to evaluate both short-term and long-term changes in water quality [18,38]. Continuous monitoring offers high-resolution data, which can help identify impacted areas and provide a comprehensive understanding of trends, including deviations from baseline conditions, particularly in remote locations where traditional monitoring efforts may be limited.

Although the available dataset was limited, the clear differences in responses at the two monitoring locations underscore the importance of integrating both short-term and long-term monitoring efforts. By deploying sondes at key monitoring locations, researchers can gain insight into wildfire-driven changes in aquatic systems and monitor these changes over extended periods. This approach has the potential to improve decision-making, inform monitoring programs, and strengthen efforts to mitigate the impacts of wildfires on aquatic ecosystems.

3.7.2. Monitoring of Water Quality Parameters

Metals, such as arsenic, cadmium, and lead, pose significant risks to aquatic systems due to their toxicity, persistence, and potential for bioaccumulation in aquatic organisms [92–94]. Even at low concentrations, metals can disrupt aquatic ecosystems by altering water chemistry, impeding the growth and reproduction of aquatic plants and animals, and entering the food chain, where they can accumulate in higher trophic levels [95,96]. Additionally, metals can bind to sediment particles, where they may remain for extended periods. The cumulative impact of metal contamination can lead to long-term impacts, underscoring the need for consistent monitoring and mitigation efforts to manage metal concentrations in wildfire-impacted water bodies.

As indicated by previous investigations [18,21,38] and this study, measuring dissolved metal concentrations in surface water is crucial for evaluating the long-term impacts associated with wildfires. While some wildfire-related contaminants decrease over time, we observed that metals remained detectable in surface water for several years after the fire event. This suggests that metals can persist in the aquatic environment, potentially affecting water quality over extended periods. By monitoring metal concentrations, we can better understand the persistence and transport of these contaminants, which is essential for assessing long-term impacts on both water and sediment quality. Long-term tracking of metals can provide valuable insights into the cumulative effects of wildfires, helping to ensure that monitoring strategies are in place to protect aquatic ecosystems from prolonged contamination.

While metals are important for evaluating long-term wildfire impacts, periodic monitoring of physical–chemical parameters is a valuable tool for identifying early signs of wildfire impacts and assessing potential effects. Parameters such as conductivity, turbidity, temperature, dissolved oxygen, and pH can respond rapidly to fire-related changes in watershed conditions, offering early indications of potential impacts before longer-term contaminant trends become evident. Consequently, both continuous monitoring and periodic sampling are important components of effective monitoring programs. Continuous measurements allow for the detection of short-term fluctuations and transient events, whereas periodic sampling provides more comprehensive insights into longer-term water quality responses. Together, these approaches support a more comprehensive assessment of wildfire impacts across multiple timescales.

In addition to these indicators, PAHs represent another critical water quality parameter essential for evaluating the impact of wildfires on aquatic systems. The compounds are toxic, persistent, and bioaccumulative contaminants, posing significant threats to both human health and the environment. Although wildfires represent an important source of PAHs in the environment, the fate of these compounds is governed by a range of physical, chemical, and biological natural attenuation processes, including biodegradation, dilution, dispersion, sorption, volatilization, and photochemical degradation [97–100].

Biodegradation represents one of the primary pathways for PAH attenuation and is strongly influenced by microbial community composition, pH, oxygen availability, temperature and nutrient levels. A variety of microorganisms, including bacteria, archaea, algae, and fungi, are capable of metabolizing PAHs by transforming them into simpler, less toxic compounds [99,101,102]. Following wildfire events, PAHs are predominantly associated with soil and sediment particulates, which limit their immediate bioavailability in the aqueous phase. As erosion and transport processes redistribute these particulates away from the source area, PAH concentrations become progressively dispersed and diluted over time. Due to their lipophilic nature and low aqueous solubility, only a fraction of PAHs partitions into the water phase. Once dissolved, PAHs may undergo photodegradation through the absorption of solar radiation, potentially producing less toxic degradation products. In the subsurface environment, volatilization losses may occur within the vadose zone, particularly for LMW 2–3 ring PAH compounds, such as naphthalene, further contributing to attenuation.

Despite the effectiveness of these natural attenuation mechanisms, even short-term elevations in PAH concentrations can result in significant and persistent risks to exposed organisms and populations. Consequently, a comprehensive understanding of the temporal dynamics governing PAH attenuation processes is essential for accurately characterizing wildfire-derived PAH inputs into aquatic systems. This knowledge is critical for effective field investigations aimed at assessing the impact of wildfire on water resources. Field program should prioritize sampling of both sediment and water matrices within the first 0–6 months following a wildfire in order to capture immediate post-fire changes in PAH composition [21,85]. Sampling during the 6 months to 2 years post-fire intervals is also necessary to evaluate the persistence and relative contribution of HMW PAHs, which degrade more slowly and can remain for extended periods.

4. Conclusions

This study demonstrates that wildfires are a significant driver of change in boreal watersheds, influencing water quality, sediment characteristics, and watershed hydrology. Across RAMP watersheds, wildfire disturbance consistently altered both the physical and chemical transport pathways that control how contaminants move through the environment. These shifts reaffirm that wildfire is not only an ecological disturbance but also a significant modifier of water resource condition and aquatic ecosystem resilience.

A key finding is that water and sediment reflect different aspects of wildfire disturbance. While water quality reflects the rapid mobilization of materials from burned landscapes, sediment provides insight into longer-term alterations in soil composition, particle redistribution, and infiltration rates. Together, these compartments reveal a linked system in which post-fire erosion, runoff, and soil destabilization act as primary mechanisms for transporting both natural and anthropogenic contaminants. This highlights the importance of integrating water and sediment monitoring when assessing cumulative wildfire impacts.

PAH compositional patterns and diagnostic ratios further show that wildfire imparts a discernible chemical signature on the landscape. However, differentiating wildfire-derived contaminants from those associated with industrial activities requires careful spatial and temporal interpretation, particularly in regions influenced by multiple, interacting stressors. PAHs, therefore, remain valuable indicators of source inputs, but their interpretation is most robust when integrated with complementary sedimentological, hydrological, and historical land disturbance data.

Hydrological modelling indicates that wildfire transforms the way watersheds partition water between infiltration, runoff, and streamflow, underscoring that hydrological change is a key component of cumulative effects. These changes reinforce the need to consider both quality and quantity in post-fire assessments, especially in regions where water supply, ecosystem services, and industrial operations depend on stable hydrologic behaviour.

Reflecting on our overall investigation, we can advise that a coordinated, multidisciplinary monitoring approach is essential for detecting early signs of wildfire disturbance, understanding ecosystem recovery, and distinguishing fire effects from other regional stressors. Strengthening partnerships among agencies, researchers, Indigenous communities, and industry will support more consistent and cohesive data collection and interpretation. Integrating fire-related parameters—such as burn severity metrics, ash-related indicators, continuous water quality sensors, and targeted contaminant analyses—into existing monitoring networks will enhance the ability to track watershed responses.

Future efforts must also include focused assessments of shallow groundwater systems with strong surface–groundwater interactions, which remain understudied yet are likely sensitive to post-fire changes in infiltration, runoff partitioning, subsurface flow pathways, and associated contaminant transport processes. Building directly on the findings of this study, ongoing follow-up initiatives expand wildfire impact assessments beyond surface water to include targeted field investigations, multiyear monitoring, and coupled surface–groundwater modelling across multiple Alberta watersheds. In parallel, advances in water quality monitoring technologies—such as electrochemical sensors and ultrasensitive nanoscale platforms—offer promising opportunities to complement established field and continuous monitoring approaches by improving sensitivity and temporal resolution for detecting wildfire-related contaminants as these technologies become more field deployable. Collectively, these efforts aim to validate the conceptual pathways identified here, quantify groundwater vulnerability and recharge responses to wildfire, and develop predictive tools and indicators that can be applied in watershed planning, post-fire response, and long-term resource management. Together, these coordinated actions can support improved early warning capacity, cumulative effects assessment, and science-based decision-making and could contribute to long-term water resource sustainability in Alberta's wildfire-prone landscapes.

Supplementary Materials: The following supporting information can be downloaded at: https://www.mdpi.com/article/10.3390/su18083771/s1, Figure S1: A spatial depiction of pre-fire conditions, burn extent, post-fire regeneration, and watershed context for the 2016 Horse River ("The Beast") Wildfire across the RAMP domain in Green Kenue™ interface, where panel (A) shows the 2015 pre-fire land-cover conditions, panel (B) illustrates the extent of the 2016 Horse River Wildfire with grey shading indicating the burned area, panel (C) presents the 2020 post-fire landscape with light-green regeneration zones dominated by early-successional grass cover, and panel (D) displays the combined map of the 2016 Horse River burn perimeter together with the RAMP watershed boundaries to highlight spatial interactions between wildfire disturbance and watershed structure; Figure S2: Box plots showing the distribution of physical–chemical parameters and metals for acid-sensitive lake water samples, categorized by site classification (R = reference, OSs = oil sands, and WF = wildfire). The central line indicates the median, the box represents the interquartile range, and the whiskers extend to values within 1.5 times the interquartile range. Outliers are shown as data points outside this range. The *y*-axis is on a logarithmic scale; Figure S3: The GRU-specific volumetric error (Dv%) as a function of GRU fractions across the calibrated 3 km domain; Table S1: List of parameters considered for water and sediment quality data; Table S2: WSC streamflow stations considered for domain-wide coarse-grid testing and targeted sub-domain calibration; Table S3: Summary of water quality parameters across the site classes. The median val-

ues are reported for each parameter, along with the number of upper outliers (UOs, values exceeding 1.5× the interquartile range above Q3) and lower outliers (LOs, values below 1.5× the interquartile range below Q1). All metals are reported in mg/L and PAHs in ng/L; Table S4: A summary of sediment quality parameters across the site classes. The median values are reported for each parameter, along with the number of upper outliers (UOs, values exceeding 1.5× the interquartile range above Q3) and lower outliers (LOs, values below 1.5× the interquartile range below Q1). All metals and PAHs are reported in mg/kg; Table S5: A summary of water quality parameters for water samples from the wildfire-affected sites, categorized by temporal variation: before (B), during (D), one year after (A1), two years after (A2), and three or more years after the fire (A3+). The median values are reported for each parameter, along with the number of upper outliers (UOs, values exceeding 1.5× the interquartile range above Q3) and lower outliers (LOs, values below 1.5× the interquartile range below Q1). All metals are reported in mg/L and PAHs in ng/L; Table S6: A summary of sediment quality parameters for sediment samples from the wildfire-affected sites, categorized by temporal variation: before (B), during (D), one year after (A1), two years after (A2), and three or more years after the fire (A3+). The median values are reported for each parameter, along with the number of upper outliers (UOs, values exceeding 1.5× the interquartile range above Q3) and lower outliers (LOs, values below 1.5× the interquartile range below Q1). All metals and PAHs are reported in mg/kg; Table S7: A summary of water quality parameters from acid-sensitive lakes quality data. The median values are reported for each parameter, along with the number of upper outliers (UOs, values exceeding 1.5× the interquartile range above Q3) and lower outliers (LOs, values below 1.5× the interquartile range below Q1). All metals are reported in mg/L; Table S8: Summary of the PAHs ratios across the site classes for water samples. The median values are reported for each parameter, along with the number of upper outliers (UOs, values exceeding 1.5× the interquartile range above Q3) and lower outliers (LOs, values below 1.5× the interquartile range below Q1); Table S9: A summary of PAH ratios across the site classes for sediment samples. The median values are reported for each parameter, along with the number of upper outliers (UOs, values exceeding 1.5× the interquartile range above Q3) and lower outliers (LOs, values below 1.5× the interquartile range below Q1); Table S10: A summary of PAH ratios for water samples from the wildfire-affected sites, categorized by temporal variation: before (B), during (D), one year after (A1), two years after (A2), and three or more years after the fire (A3+). The median values are reported for each parameter, along with the number of upper outliers (UOs, values exceeding 1.5× the interquartile range above Q3) and lower outliers (LOs, values below 1.5× the interquartile range below Q1); Table S11: A summary of PAH ratios across for sediment samples from the wildfire-affected sites, categorized by temporal variation: before (B), during (D), one year after (A1), two years after (A2), and three or more years after the fire (A3+). The median values are reported for each parameter, along with the number of upper outliers (UOs, values exceeding 1.5× the interquartile range above Q3) and lower outliers (LOs, values below 1.5× the interquartile range below Q1); Table S12: Model performance metrics across hydrometric stations and domain configurations.

Author Contributions: Conceptualization, D.W., T.A.M., A.J., M.W., T.S., J.J.G. and N.K.; methodology, D.W., T.A.M., A.J., M.W., T.S., J.J.G. and N.K.; software, D.W. and N.K.; validation, D.W., T.A.M., A.J., M.W., T.S., J.J.G. and N.K.; formal analysis, D.W., T.A.M., N.K. and A.J.; investigation, D.W., T.A.M., N.K. and A.J.; resources, D.W., T.A.M., A.J., M.W., T.S., J.J.G. and N.K.; data curation, D.W., T.A.M., N.K. and A.J.; writing—original draft preparation, D.W., T.A.M. and A.J.; writing—review and editing, D.W., T.A.M., A.J., M.W., T.S., J.J.G. and N.K.; visualization, D.W., T.A.M., N.K. and A.J.; supervision, J.J.G. and N.K.; project administration, D.W.; funding acquisition, D.W., A.J., M.W., T.S. and J.J.G. All authors have read and agreed to the published version of the manuscript.

Funding: This research was funded by InnoTech Alberta Inc.'s Strategic Investment Grant, grant numbers ENV-2023-IN-059 and ENV-2025-IN-037.

Institutional Review Board Statement: Not applicable.

Informed Consent Statement: Not applicable.

Data Availability Statement: All data used in this study are available in the Supplementary Materials. Legacy RAMP datasets (http://www.ramp-alberta.org/RAMP.aspx; accessed on 28 March 2024) are publicly archived in the Oil Sands Monitoring (OSM) Data Catalogue and will remain accessible after the RAMP website is decommissioned in early 2026: https://osmdatacatalog.alberta.ca/pubdata/ramp-website accessed on 28 March 2024.

Acknowledgments: We thank Jean Birks and Mike C. Moncur for their instrumental contributions to the conceptualization of the initial proposal.

Conflicts of Interest: All authors declare that the research was conducted in the absence of any commercial or financial relationships that could be construed as a potential conflict of interest.

Abbreviations

The following abbreviations are used in this manuscript:

PAHs	Polycyclic Aromatic Hydrocarbons
SRWP	Southern Rockies Watershed Program
RAMP	Regional Aquatics Monitoring Program
LTRN	Long-Term River Network
OSM	Oil Sands Monitoring
DO	Dissolved Oxygen
TSSs	Total Suspended Solids
TOC	Total Organic Carbon
LMW PAHs	Light-Molecular Weight PAHs
HMW PAHs	High-Molecular Weight PAHs
CCME	Canadian Council of Ministers of the Environment
PI	Pyrogenic Index
GRUs	Grouped Response Units
LULC	Land-Use/Land-Cover
MRDEM	Medium Resolution Digital Elevation Model
NRCan	Natural Resources Canada
RDPA–CaPA	Regional Deterministic Precipitation Analysis–Canadian Precipitation Analysis
RDPS	Regional Deterministic Prediction System
ECCC	Environment and Climate Change Canada
WSC	Water Survey of Canada
RDRS	Regional Deterministic Reanalysis System
DDS	Dynamically Dimensioned Search
KGE	Kling–Gupta Efficiency
NSE	Nash–Sutcliffe Efficiency

References

1. UNDRR. The Invisible Costs of Wildfire Disasters in 2025. Available online: https://www.undrr.org/news/invisible-costs-wildfire-disasters-2025 (accessed on 23 March 2026).
2. Government of Canada, S.C. Measuring the Economic Cost of Wildfires. Available online: https://www.statcan.gc.ca/o1/en/plus/8369-measuring-economic-cost-wildfires (accessed on 23 March 2026).
3. Canadian Interagency Forest Fire Centre (CIFFC). *National Wildland Fire Situation Report: 2023 Summary*; Canadian Interagency Forest Fire Centre: Winnipeg, MB, Canada, 2024.
4. Severe Weather in 2023 Caused Over $3.1 Billion in Insured Damage. Available online: https://www.ibc.ca/news-insights/news/severe-weather-in-2023-caused-over-3-1-billion-in-insured-damage (accessed on 23 March 2026).
5. Bladon, K.D.; Emelko, M.B.; Silins, U.; Stone, M. Wildfire and the Future of Water Supply. *Environ. Sci. Technol.* **2014**, *48*, 8936–8943. [CrossRef] [PubMed]
6. Canada's Wildfire Crisis: Economic & Trade Disruption. Available online: https://www.edc.ca/en/article/2025-wildfires-impact-canadian-trade.html (accessed on 23 March 2026).

7. U.S. Geological Survey. Water Quality After Wildfire. Available online: https://www.usgs.gov/mission-areas/water-resources/science/water-quality-after-wildfire (accessed on 23 March 2026).
8. Murphy, P.J. *History of Forest and Prairie Fire Control Policy in Alberta*; Alberta Energy and Natural Resources: Edmonton, Alberta, 1985.
9. Alberta Forestry and Parks. *Historical Wildfire Database and Spatial Wildfire Data: Data Dictionary (2006–2025)*; Government of Alberta: Edmonton, AB, Canada, 2026. Available online: https://open.alberta.ca/dataset/a221e7a0-4f46-4be7-9c5a-e29de9a3447e/resource/1b635b8b-a937-4be4-857e-8aeef77365d2/download/fp-historical-wildfire-data-dictionary-2006-2025.pdf (accessed on 30 March 2026).
10. Ahmed, M.R.; Hassan, Q.K. Occurrence, Area Burned, and Seasonality Trends of Forest Fires in the Natural Subregions of Alberta over 1959–2021. *Fire* **2023**, *6*, 96. [CrossRef]
11. Luo, B.; Luo, D.; Dai, A.; Xiao, C.; Simmonds, I.; Hanna, E.; Overland, J.; Shi, J.; Chen, X.; Yao, Y.; et al. Rapid Summer Russian Arctic Sea-Ice Loss Enhances the Risk of Recent Eastern Siberian Wildfires. *Nat. Commun.* **2024**, *15*, 5399. [CrossRef] [PubMed]
12. Johnk, B.T.; Mays, D.C. Wildfire Impacts on Groundwater Aquifers: A Case Study of the 1996 Honey Boy Fire in Beaver County, Utah, USA. *Water* **2021**, *13*, 2279. [CrossRef]
13. Mastrorillo, L.; Mazza, R.; Viaroli, S. Recharge Process of a Dune Aquifer (Roman Coast, Italy). *Acque Sotter. Ital. J. Groundw.* **2018**, *7*. [CrossRef]
14. Mansilha, C.; Carvalho, A.; Guimarães, P.; Espinha Marques, J. Water Quality Concerns Due to Forest Fires: Polycyclic Aromatic Hydrocarbons (PAH) Contamination of Groundwater from Mountain Areas. *J. Toxicol. Environ. Health Part A* **2014**, *77*, 806–815. [CrossRef]
15. Verma, S.; Jayakumar, S. Impact of Forest Fire on Physical, Chemical and Biological Properties of Soil: A Review. *Proc. Int. Acad. Ecol. Environ. Sci.* **2012**, *2*, 168.
16. Petach, T. Impacts of Wildfire Ash Leachate on Transport of Cryptosporidium Parvum Oocysts Through Porous Media. Master's Thesis, Cornell University, New York, NY, USA, 2018. [CrossRef]
17. Inbar, M.; Tamir, M.; Wittenberg, L. Runoff and Erosion Processes after a Forest Fire in Mount Carmel, a Mediterranean Area. *Geomorphology* **1998**, *1*, 17–33. [CrossRef]
18. Emmerton, C.A.; Cooke, C.A.; Hustins, S.; Silins, U.; Emelko, M.B.; Lewis, T.; Kruk, M.K.; Taube, N.; Zhu, D.; Jackson, B.; et al. Severe Western Canadian Wildfire Affects Water Quality Even at Large Basin Scales. *Water Res.* **2020**, *183*, 116071. [CrossRef]
19. Raoelison, O.D.; Valenca, R.; Lee, A.; Karim, S.; Webster, J.P.; Poulin, B.A.; Mohanty, S.K. Wildfire Impacts on Surface Water Quality Parameters: Cause of Data Variability and Reporting Needs. *Environ. Pollut.* **2023**, *317*, 120713. [CrossRef]
20. Rust, A.J.; Hogue, T.S.; Saxe, S.; McCray, J. Post-Fire Water-Quality Response in the Western United States. *Int. J. Wildland Fire* **2018**, *3*, 203–216. [CrossRef]
21. Paul, M.J.; LeDuc, S.D.; Lassiter, M.G.; Moorhead, L.C.; Noyes, P.D.; Leibowitz, S.G. Wildfire Induces Changes in Receiving Waters: A Review with Considerations for Water Quality Management. *Water Resour. Res.* **2022**, *58*, e2021WR030699. [CrossRef] [PubMed]
22. Murphy, S.F.; McCleskey, R.B.; Martin, D.A.; Holloway, J.M.; Writer, J.H. Wildfire-Driven Changes in Hydrology Mobilize Arsenic and Metals from Legacy Mine Waste. *Sci. Total Environ.* **2020**, *743*, 140635. [CrossRef] [PubMed]
23. Caldwell, P.V.; Elliott, K.J.; Liu, N.; Vose, J.M.; Zietlow, D.R.; Knoepp, J.D. Watershed-scale Vegetation, Water Quantity, and Water Quality Responses to Wildfire in the Southern Appalachian Mountain Region, United States. *Hydrol. Process.* **2020**, *34*, 5188–5209. [CrossRef]
24. Loiselle, D.; Du, X.; Alessi, D.S.; Bladon, K.D.; Faramarzi, M. Projecting Impacts of Wildfire and Climate Change on Streamflow, Sediment, and Organic Carbon Yields in a Forested Watershed. *J. Hydrol.* **2020**, *590*, 125403. [CrossRef]
25. Williams, A.P.; Livneh, B.; McKinnon, K.A.; Hansen, W.D.; Mankin, J.S.; Cook, B.I.; Smerdon, J.E.; Varuolo-Clarke, A.M.; Bjarke, N.R.; Juang, C.S.; et al. Growing Impact of Wildfire on Western US Water Supply. *Proc. Natl. Acad. Sci. USA* **2022**, *119*, e2114069119. [CrossRef]
26. Williams, C.H.; Silins, U.; Spencer, S.A.; Wagner, M.J.; Stone, M.; Emelko, M.B. Net Precipitation in Burned and Unburned Subalpine Forest Stands after Wildfire in the Northern Rocky Mountains. *Int. J. Wildland Fire* **2019**, *28*, 750–760. [CrossRef]
27. Puntenney-Desmond, K.C.; Bladon, K.D.; Silins, U. Runoff and Sediment Production from Harvested Hillslopes and the Riparian Area during High Intensity Rainfall Events. *J. Hydrol.* **2020**, *582*, 124452. [CrossRef]
28. Collins, A.L.; Blackwell, M.; Boeckx, P.; Chivers, C.-A.; Emelko, M.; Evrard, O.; Foster, I.; Gellis, A.; Gholami, H.; Granger, S. Sediment Source Fingerprinting: Benchmarking Recent Outputs, Remaining Challenges and Emerging Themes. *J. Soils Sediments* **2020**, *20*, 4160–4193. [CrossRef]
29. Spencer, S.A.; Anderson, A.E.; Silins, U.; Collins, A.L. Hillslope and Groundwater Contributions to Streamflow in a Rocky Mountain Watershed Underlain by Glacial till and Fractured Sedimentary Bedrock. *Hydrol. Earth Syst. Sci.* **2021**, *25*, 237–255. [CrossRef]

30. Martens, A.M.; Silins, U.; Proctor, H.C.; Williams, C.H.; Wagner, M.J.; Emelko, M.B.; Stone, M. Long-Term Impact of Severe Wildfire and Post-Wildfire Salvage Logging on Macroinvertebrate Assemblage Structure in Alberta's Rocky Mountains. *Int. J. Wildland Fire* **2019**, *28*, 738–749. [CrossRef]
31. Rhoades, C.C.; Nunes, J.P.; Silins, U.; Doerr, S.H. The Influence of Wildfire on Water Quality and Watershed Processes: New Insights and Remaining Challenges. *Int. J. Wildland Fire* **2019**, *28*, 721–725. [CrossRef]
32. McEachern, P.; Prepas, E.E.; Gibson, J.J.; Dinsmore, W.P. Forest Fire Induced Impacts on Phosphorus, Nitrogen, and Chlorophyll a Concentrations in Boreal Subarctic Lakes of Northern Alberta. *Can. J. Fish. Aquat. Sci.* **2000**, *57*, 73–81. [CrossRef]
33. Wagner, M.J.; Bladon, K.D.; Silins, U.; Williams, C.H.; Martens, A.M.; Boon, S.; MacDonald, R.J.; Stone, M.; Emelko, M.B.; Anderson, A. Catchment-Scale Stream Temperature Response to Land Disturbance by Wildfire Governed by Surface–Subsurface Energy Exchange and Atmospheric Controls. *J. Hydrol.* **2014**, *517*, 328–338. [CrossRef]
34. Brandt, J.P.; Flannigan, M.D.; Maynard, D.G.; Thompson, I.D.; Volney, W.J.A. An Introduction to Canada's Boreal Zone: Ecosystem Processes, Health, Sustainability, and Environmental Issues. *Environ. Rev.* **2013**, *21*, 207–226. [CrossRef]
35. Nwaishi, F.; Morison, M.; Plach, J.; Macrae, M.; Petrone, R. Carbon and Nutrient Stoichiometric Relationships in the Soil–Plant Systems of Disturbed Boreal Forest Peatlands within Athabasca Oil Sands Region, Canada. *Forests* **2022**, *13*, 865. [CrossRef]
36. Atkinson, N. Landscapes of the Alberta Oil Sands. In *Landscapes and Landforms of Western Canada*; Slaymaker, O., Ed.; World Geomorphological Landscapes; Springer International Publishing: Cham, Switzerland, 2017; pp. 395–410.
37. Pickell, P.D.; Andison, D.W.; Coops, N.C. Characterizations of Anthropogenic Disturbance Patterns in the Mixedwood Boreal Forest of Alberta, Canada. *For. Ecol. Manag.* **2013**, *304*, 243–253. [CrossRef]
38. Murphy, S.F.; Alpers, C.N.; Anderson, C.W.; Banta, J.R.; Blake, J.M.; Carpenter, K.D.; Clark, G.D.; Clow, D.W.; Hempel, L.A.; Martin, D.A.; et al. A Call for Strategic Water-Quality Monitoring to Advance Assessment and Prediction of Wildfire Impacts on Water Supplies. *Front. Water* **2023**, *5*, 1144225. [CrossRef]
39. Singh, R.K.; Singh, S.K. Persistent Polycyclic Aromatic Hydrocarbons (PAHs) in the Soil, Its Bioremediation, and Health Effects. *Environ. Sci. Eur.* **2025**, *37*, 187. [CrossRef]
40. Patel, A.B.; Shaikh, S.; Jain, K.R.; Desai, C.; Madamwar, D. Polycyclic Aromatic Hydrocarbons: Sources, Toxicity, and Remediation Approaches. *Front. Microbiol.* **2020**, *11*, 562813. [CrossRef]
41. Montano, L.; Baldini, G.M.; Piscopo, M.; Liguori, G.; Lombardi, R.; Ricciardi, M.; Esposito, G.; Pinto, G.; Fontanarosa, C.; Spinelli, M. Polycyclic Aromatic Hydrocarbons (PAHs) in the Environment: Occupational Exposure, Health Risks and Fertility Implications. *Toxics* **2025**, *13*, 151. [CrossRef]
42. CCME (Canadian Council of Ministers of the Environment). Appendix IX—A protocol for the derivation of water quality guidelines for the protection of aquatic life (April 1991). In *Canadian Water Quality Guidelines*; Canadian Council of Ministers of the Environment: Winnipeg, MB, Canada, 1991.
43. Abdel-Shafy, H.I.; Mansour, M.S. A Review on Polycyclic Aromatic Hydrocarbons: Source, Environmental Impact, Effect on Human Health and Remediation. *Egypt. J. Pet.* **2016**, *25*, 107–123. [CrossRef]
44. Berríos-Rolón, P.J.; Cotto, M.; Márquez, F. Polycyclic Aromatic Hydrocarbons (PAHs) in Freshwater Systems: A Comprehensive Review of Sources, Distribution, and Impacts. *Toxics* **2025**, *13*, 321. [CrossRef] [PubMed]
45. Jafarabadi, A.R.; Dashtbozorg, M.; Mitra, S.; Bakhtiari, A.R.; Dehkordi, S.M.; Cappello, T. Historical Sedimentary Deposition and Ecotoxicological Impact of Aromatic Biomarkers in Sediment Cores from Ten Coral Reefs of the Persian Gulf, Iran. *Sci. Total Environ.* **2019**, *696*, 133969. [CrossRef] [PubMed]
46. Wakeham, S.G.; Canuel, E.A. Biogenic Polycyclic Aromatic Hydrocarbons in Sediments of the San Joaquin River in California (USA), and Current Paradigms on Their Formation. *Environ. Sci. Pollut. Res.* **2016**, *23*, 10426–10442. [CrossRef]
47. Buczyńska, A.J.; Geypens, B.; Van Grieken, R.; De Wael, K. Stable Carbon Isotopic Ratio Measurement of Polycyclic Aromatic Hydrocarbons as a Tool for Source Identification and Apportionment—A Review of Analytical Methodologies. *Talanta* **2013**, *105*, 435–450. [CrossRef] [PubMed]
48. O'Malley, K.E.; Ghetu, C.C.; Rohlman, D.; Anderson, K.A. Assessing Wildfire Impact on Diffusive Flux of Parent and Alkylated PAHs: A Pilot Study of Soil–Air Chemical Movement before, during, and after Wildfires. *Environ. Sci. Technol.* **2024**, *58*, 23117–23126. [CrossRef]
49. Kieta, K.A.; Owens, P.N.; Petticrew, E.L.; French, T.D.; Koiter, A.J.; Rutherford, P.M. Polycyclic Aromatic Hydrocarbons in Terrestrial and Aquatic Environments Following Wildfire: A Review. *Environ. Rev.* **2022**, *31*, 141–167. [CrossRef]
50. Goto, Y.; Nakamuta, K.; Nakata, H. Parent and Alkylated PAHs Profiles in 11 Petroleum Fuels and Lubricants: Application for Oil Spill Accidents in the Environment. *Ecotoxicol. Environ. Saf.* **2021**, *224*, 112644. [CrossRef]
51. Stogiannidis, E.; Laane, R. Source Characterization of Polycyclic Aromatic Hydrocarbons by Using Their Molecular Indices: An Overview of Possibilities. *Rev. Environ. Contam. Toxicol.* **2014**, *234*, 49–133.

52. Gao, P.; Li, H.; Wilson, C.P.; Townsend, T.G.; Xiang, P.; Liu, Y.; Ma, L.Q. Source Identification of PAHs in Soils Based on Stable Carbon Isotopic Signatures. *Crit. Rev. Environ. Sci. Technol.* **2018**, *48*, 923–948. [CrossRef]
53. Wang, Z.; Yang, C.; Parrott, J.L.; Frank, R.A.; Yang, Z.; Brown, C.E.; Hewitt, L.M. Forensic Source Differentiation of Petrogenic, Pyrogenic, and Biogenic Hydrocarbons in Canadian Oil Sands Environmental Samples. *J. Hazard. Mater.* **2014**, *271*, 166–177. [CrossRef] [PubMed]
54. Wang, D.G.; Yang, M.; Jia, H.L.; Zhou, L.; Li, Y.F. Polycyclic Aromatic Hydrocarbons in Urban Street Dust and Surface Soil: Comparisons of Concentration, Profile, and Source. *Arch. Environ. Contam. Toxicol.* **2009**, *56*, 173–180. [CrossRef]
55. Kim, D.; Kumfer, B.M.; Anastasio, C.; Kennedy, I.M.; Young, T.M. Environmental Aging of Polycyclic Aromatic Hydrocarbons on Soot and Its Effect on Source Identification. *Chemosphere* **2009**, *76*, 1075–1081. [CrossRef] [PubMed]
56. Zhang, X.L.; Tao, S.; Liu, W.X.; Yang, Y.; Zuo, Q.; Liu, S.Z. Source Diagnostics of Polycyclic Aromatic Hydrocarbons Based on Species Ratios: A Multimedia Approach. *Environ. Sci. Technol.* **2005**, *39*, 9109–9114. [CrossRef]
57. Walvoord, M.A.; Ebel, B.A.; Partridge, T.F.; Rey, D.M.; Rosenberry, D.O. Disparate Groundwater Responses to Wildfire. *WIREs Water* **2025**, *12*, e70029. [CrossRef]
58. Bolotin, L.A.; McMillan, H. A Hydrologic Signature Approach to Analysing Wildfire Impacts on Overland Flow. *Hydrol. Process.* **2024**, *38*, e15215. [CrossRef]
59. Nyman, P.; Sheridan, G.J.; Smith, H.G.; Lane, P.N. Modeling the Effects of Surface Storage, Macropore Flow and Water Repellency on Infiltration after Wildfire. *J. Hydrol.* **2014**, *513*, 301–313. [CrossRef]
60. Ebel, B.A.; Hammond, J.C.; Walvoord, M.; Partridge, T.F.; Rey, D.; Murphy, S.F. A Review and Synthesis of Post-Wildfire Shifts in Hydrologic Processes and Streamflow Generation Mechanisms. *Environ. Res. Water* **2026**, *1*, 042001. [CrossRef]
61. Ebel, B.A.; Shephard, Z.M.; Walvoord, M.A.; Murphy, S.F.; Partridge, T.F.; Perkins, K.S. Modeling Post-Wildfire Hydrologic Response: Review and Future Directions for Applications of Physically Based Distributed Simulation. *Earth's Future* **2023**, *11*, e2022EF003038. [CrossRef]
62. Introduction to WATFLOOD. Available online: https://www.civil.uwaterloo.ca/watflood/intro/intro.htm (accessed on 26 January 2026).
63. Kouwen, N.; Soulis, E.; Pietroniro, A.; Donald, J.; Harrington, R. Grouped Response Units for Distributed Hydrologic Modeling. *J. Water Resour. Plan. Manag.* **1993**, *119*, 289–305. [CrossRef]
64. WATFLOOD. Available online: http://www.watflood.ca/ (accessed on 26 January 2026).
65. Canada, N.R.C. Green Kenue™: Software Tool for Hydrologic Modellers. Available online: https://nrc.canada.ca/en/research-development/products-services/software-applications/green-kenuetm-software-tool-hydrologic-modellers (accessed on 26 January 2026).
66. Canada, N.R. Medium Resolution Digital Elevation Model (MRDEM)—CanElevation Series—Open Government Portal. Available online: https://open.canada.ca/data/en/dataset/18752265-bda3-498c-a4ba-9dfe68cb98da (accessed on 23 January 2026).
67. Canada, N.R. 2015 Land Cover of Canada—Open Government Portal. Available online: https://open.canada.ca/data/en/dataset/4e615eae-b90c-420b-adee-2ca35896caf6 (accessed on 23 January 2026).
68. Canada, N.R. 2020 Land Cover of Canada—Open Government Portal. Available online: https://open.canada.ca/data/dataset/ee1580ab-a23d-4f86-a09b-79763677eb47 (accessed on 23 January 2026).
69. Fortin, V.; Roy, G.; Stadnyk, T.; Koenig, K.; Gasset, N.; Mahidjiba, A. Ten Years of Science Based on the Canadian Precipitation Analysis: A CaPA System Overview and Literature Review. *Atmos.-Ocean* **2018**, *56*, 178–196. [CrossRef]
70. Tolson, B.A.; Shoemaker, C.A. Efficient Prediction Uncertainty Approximation in the Calibration of Environmental Simulation Models. *Water Resour. Res.* **2008**, *44*, 2007WR005869. [CrossRef]
71. Matott, L.S. *OSTRICH–An Optimization Software Toolkit for Research Involving Computational Heuristics; Documentation and User's Guide, Version 17.12.19*; State University of New York at Buffalo: Buffalo, NY, USA, 2019; Available online: https://www.civil.uwaterloo.ca/jrcraig/CIVE781/Ostrich_Manual_17_12_19.pdf (accessed on 30 March 2026).
72. Kling, H.; Fuchs, M.; Paulin, M. Runoff Conditions in the Upper Danube Basin under an Ensemble of Climate Change Scenarios. *J. Hydrol.* **2012**, *424*, 264–277. [CrossRef]
73. Gupta, H.V.; Kling, H.; Yilmaz, K.K.; Martinez, G.F. Decomposition of the Mean Squared Error and NSE Performance Criteria: Implications for Improving Hydrological Modelling. *J. Hydrol.* **2009**, *377*, 80–91. [CrossRef]
74. Waseem, M.; Mani, N.; Andiego, G.; Usman, M. A Review of Criteria of Fit for Hydrological Models. *Int. Res. J. Eng. Technol.* **2017**, *4*, 1765–1772.
75. Kouwen, N.; Danard, M.; Bingeman, A.; Luo, W.; Seglenieks, F.R.; Soulis, E.D. Case Study: Watershed Modeling with Distributed Weather Model Data. *J. Hydrol. Eng.* **2005**, *10*, 23–38. [CrossRef]
76. Singh, S.K.; Pahlow, M.; Booker, D.J.; Shankar, U.; Chamorro, A. Towards Baseflow Index Characterisation at National Scale in New Zealand. *J. Hydrol.* **2019**, *568*, 646–657. [CrossRef]

77. Arocena, J.M.; Opio, C. Prescribed Fire-Induced Changes in Properties of Sub-Boreal Forest Soils. *Geoderma* **2003**, *113*, 1–16. [CrossRef]
78. Moody, J.A.; Shakesby, R.A.; Robichaud, P.R.; Cannon, S.H.; Martin, D.A. Current Research Issues Related to Post-Wildfire Runoff and Erosion Processes. *Earth-Sci. Rev.* **2013**, *122*, 10–37. [CrossRef]
79. Burton, C.A.; Hoefen, T.M.; Plumlee, G.S.; Baumberger, K.L.; Backlin, A.R.; Gallegos, E.; Fisher, R.N. Trace Elements in Stormflow, Ash, and Burned Soil Following the 2009 Station Fire in Southern California. *PLoS ONE* **2016**, *5*, e0153372. [CrossRef] [PubMed]
80. Campo, J.; Lorenzo, M.; Cammeraat, E.L.H.; Picó, Y.; Andreu, V. Emerging Contaminants Related to the Occurrence of Forest Fires in the Spanish Mediterranean. *Sci. Total Environ.* **2017**, *603*, 330–339. [CrossRef] [PubMed]
81. Klimas, K.; Hiesl, P.; Hagan, D.; Park, D. Prescribed Fire Effects on Sediment and Nutrient Exports in Forested Environments: A Review. *J. Environ. Qual.* **2020**, *4*, 793–811. [CrossRef] [PubMed]
82. Homann, J.; Karbach, N.; Carolin, S.A.; James, D.H.; Hodell, D.; Breitenbach, S.F.; Hoffmann, T. Past Fire Dynamics Inferred from Polycyclic Aromatic Hydrocarbons and Monosaccharide Anhydrides in a Stalagmite from the Archaeological Site of Mayapan, Mexico. *Biogeosciences* **2023**, *20*, 3249–3260. [CrossRef]
83. Yunker, M.B.; Macdonald, R.W.; Vingarzan, R.; Mitchell, R.H.; Goyette, D.; Sylvestre, S. PAHs in the Fraser River Basin: A Critical Appraisal of PAH Ratios as Indicators of PAH Source and Composition. *Org. Geochem.* **2002**, *33*, 489–515. [CrossRef]
84. Yan, B.; Abrajano, T.A.; Bopp, R.F.; Chaky, D.A.; Benedict, L.A.; Chillrud, S.N. Molecular Tracers of Saturated and Polycyclic Aromatic Hydrocarbon Inputs into Central Park Lake, New York City. *Environ. Sci. Technol.* **2005**, *39*, 7012–7019. [CrossRef]
85. Campos, I.; Abrantes, N.; Pereira, P.; Micaelo, A.C.; Vale, C.; Keizer, J.J. Forest Fires as Potential Triggers for Production and Mobilization of Polycyclic Aromatic Hydrocarbons to the Terrestrial Ecosystem. *Land Degrad. Dev.* **2019**, *30*, 2360–2370. [CrossRef]
86. Sprovieri, M.; Feo, M.L.; Prevedello, L.; Manta, D.S.; Sammartino, S.; Marsella, E. Heavy Metals, Polycyclic Aromatic Hydrocarbons and Polychlorinated Biphenyls in Surface Sediments of the Naples Harbour (Southern Italy). *Chemosphere* **2007**, *67*, 998–1009. [CrossRef]
87. Smith, H.G.; Sheridan, G.J.; Lane, P.N.J.; Noske, P.J.; Heijnis, H. Changes to Sediment Sources Following Wildfire in a Forested Upland Catchment, Southeastern Australia. *Hydrol. Process.* **2011**, *25*, 2878–2889. [CrossRef]
88. Choi, S.-D.; Shunthirasingham, C.; Daly, G.L.; Xiao, H.; Lei, Y.D.; Wania, F. Levels of Polycyclic Aromatic Hydrocarbons in Canadian Mountain Air and Soil Are Controlled by Proximity to Roads. *Environ. Pollut.* **2009**, *157*, 3199–3206. [CrossRef]
89. Ding, X.; Wang, X.-M.; Xie, Z.-Q.; Xiang, C.-H.; Mai, B.-X.; Sun, L.-G.; Zheng, M.; Sheng, G.-Y.; Fu, J.-M.; Pöschl, U. Atmospheric Polycyclic Aromatic Hydrocarbons Observed over the North Pacific Ocean and the Arctic Area: Spatial Distribution and Source Identification. *Atmos. Environ.* **2007**, *41*, 2061–2072. [CrossRef]
90. Kouwen, N. *WATFLOOD^{TM}—Model Setup for MRBHM Update: Final Report*; Government of the Northwest Territories: Yellowknife, NT, Canada, 2016.
91. Jenkinson, R.W. Surface Water Quality Modelling Considering Riparian Wetlands. Doctoral dissertation, University of Waterloo, Waterloo, ON, Canada, 2009.
92. Ali, H.; Khan, E. Trophic Transfer, Bioaccumulation, and Biomagnification of Non-Essential Hazardous Heavy Metals and Metalloids in Food Chains/Webs—Concepts and Implications for Wildlife and Human Health. *Hum. Ecol. Risk Assess. Int. J.* **2019**, *25*, 1353–1376. [CrossRef]
93. Sharma, M.; Kant, R.; Sharma, A.K.; Sharma, A.K. Exploring the Impact of Heavy Metals Toxicity in the Aquatic Ecosystem. *Int. J. Energy Water Resour.* **2024**, *9*, 267–280. [CrossRef]
94. Subhanullah, M.; Hassan, N.; Ali, S.; Saleh, I.A.; Ilyas, M.; Rawan, B.; Ullah, W.; Iqbal, B.; Okla, M.K.; Alaraidh, I.A.; et al. The Detrimental Effects of Heavy Metals on Tributaries Exert Pressure on Water Quality, Crossocheilus Aplocheilus, and the Well-Being of Human Health. *Sci. Rep.* **2024**, *14*, 2868. [CrossRef] [PubMed]
95. Briffa, J.; Sinagra, E.; Blundell, R. Heavy Metal Pollution in the Environment and Their Toxicological Effects on Humans. *Heliyon* **2020**, *6*, e04691. [CrossRef]
96. Shahjahan, M.; Taslima, K.; Rahman, M.S.; Al-Emran, M.D.; Alam, S.I.; Faggio, C. Effects of Heavy Metals on Fish Physiology–A Review. *Chemosphere* **2022**, *300*, 134519. [CrossRef]
97. Haritash, A.K.; Kaushik, C.P. Biodegradation Aspects of Polycyclic Aromatic Hydrocarbons (PAHs): A Review. *J. Hazard. Mater.* **2009**, *169*, 1–15. [CrossRef]
98. Bertilsson, S.; Widenfalk, A. Photochemical Degradation of PAHs in Freshwaters and Their Impact on Bacterial Growth–Influence of Water Chemistry. *Hydrobiologia* **2002**, *469*, 23–32. [CrossRef]
99. Rogers, S.W.; Ong, S.K.; Kjartanson, B.H.; Golchin, J.; Stenback, G.A. Natural Attenuation of Polycyclic Aromatic Hydrocarbon-Contaminated Sites. *Pract. Period. Hazard. Toxic Radioact. Waste Manag.* **2002**, *6*, 141–155. [CrossRef]
100. Miller, J.S.; Olejnik, D. Photolysis of Polycyclic Aromatic Hydrocarbons in Water. *Water Res.* **2001**, *35*, 233–243. [CrossRef]

101. Yu, K.S.H.; Wong, A.H.Y.; Yau, K.W.Y.; Wong, Y.S.; Tam, N.F.Y. Natural Attenuation, Biostimulation and Bioaugmentation on Biodegradation of Polycyclic Aromatic Hydrocarbons (PAHs) in Mangrove Sediments. *Mar. Pollut. Bull.* **2005**, *51*, 1071–1077. [CrossRef] [PubMed]
102. Ramsay, M.A.; Swannell, R.P.; Shipton, W.A.; Duke, N.C.; Hill, R.T. Effect of Bioremediation on the Microbial Community in Oiled Mangrove Sediments. *Mar. Pollut. Bull.* **2000**, *41*, 413–419. [CrossRef]

Disclaimer/Publisher's Note: The statements, opinions and data contained in all publications are solely those of the individual author(s) and contributor(s) and not of MDPI and/or the editor(s). MDPI and/or the editor(s) disclaim responsibility for any injury to people or property resulting from any ideas, methods, instructions or products referred to in the content.